Supporting Information

Cobalt-Bridged Secondary Building Units in a Titanium Metal-Organic Framework for Cascade Reduction of *N*-heteroarenes

Xuanyu Feng,[†,1] Yang Song,[†,1] Justin S. Chen,[1] Zhe Li,[1,2] Emily Y. Chen,[1] Michael Kaufmann,[1] Cheng Wang,[2] and Wenbin Lin*[,1,2]

[1]Department of Chemistry, The University of Chicago, 929 E 57th St, Chicago, IL 60637, USA

[2]College of Chemistry and Chemical Engineering, iCHEM, State Key Laboratory of Physical Chemistry of Solid Surface, Xiamen University, Xiamen 361005, China

E-mail: wenbinlin@uchicago.edu

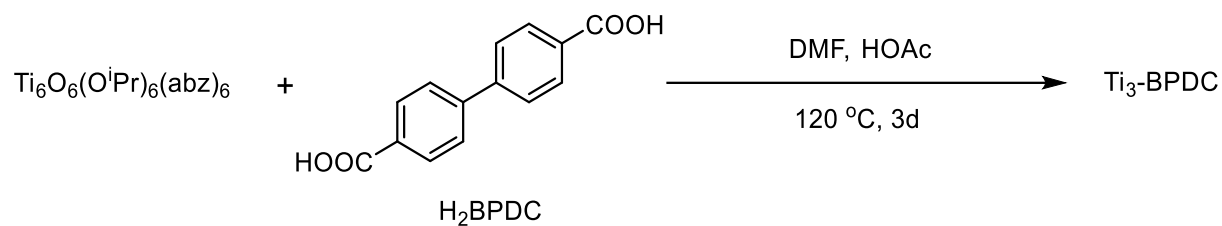| Contents	Page

1. A List of Reported Ti-carboxylate MOFs

Table S1. A complete list of known Ti-carboxylate MOFs

Name	Molecular formula	Organic linker (L)	Inorganic unit nuclearity	Network dimensionality	Porosity	Reported year
MIL-125	$Ti_8O_8(OH)_4(L)_6$	Terephthalate	8	3-D	$S_{BET}=1150$ m^2/g (N$_2$ 77 K)	2009[1]
NTU-9	$Ti_2(H-L)_2(H_2-L)_n$	2,5-Dihydroxyterephthalate	1	2-D	---	2014[2]
COK-69	$Ti_3O_3(L)_3 \cdot DMF$	1,4-Cyclohexane dicarboxylate	3	3-D	$S_{BET}=29$ m^2/g (N$_2$ 77 K)	2015[3]
MIL-101(Ti)	$Ti_3O(OEt)(L)_3$	Terephthalate	3	3-D	$S_{BET}=2970$ m^2/g (N$_2$ 77 K)	2015[4]
PCN-22	$Ti_7O_6(L)_{12} \cdot 2(DEF)$	Tetrakis(4-carboxyphenyl) porphyrin	7	3-D	$S_{BET}=1284$ m^2/g (N$_2$ 77 K)	2015[5]
MIL-167	$Ti(L)_{1.5}(Et_2MeNH)_2 \cdot n H_2O$	2,5-Dihydroxyterephthalate	1	3-D	---	2016[6]
MIL-168	$Ti(L)(cat) \cdot 2DEAH$	2,5-Dihydroxyterephthalate	1	1-D	---	2016[6]
MIL-169	$TiO_{0.5}(L)(H_2O)(H_2-pip)_{0.5} \cdot nH_2O$	2,5-Dihydroxyterephthalate	1	2-D	---	2016[6]
MOF-901	$Ti_6O_6(OMe)_6(L)_3$	1,4-Phenylenebis(methanylylidene)bis(azanylylidene)dibenzoate	6	2-D	$S_{BET}=550$ m^2/g (N$_2$ 77 K)	2016[7]
MOF-902	$Ti_6O_6(OMe)_6(L)_3$	Biphenyl-4,4-diylbis-(methanylylidene)bis(azanylylidene)dibenzoate	6	2-D	$S_{BET}=400$ m^2/g (N$_2$ 77 K)	2017[8]
MIL-177-LT	$Ti_{12}O_{15}(mdip)_3(formate)_6$	3,3',5,5'-tetra-carboxydiphenylmethane	12	3-D	$S_{BET}=730$ m^2/g (N$_2$ 77 K)	2018[9]
DGIST-1	$Ti_2(\mu_2-O)_2(L)$	Tetrakis(4-carboxyphenyl) porphyrin	2D-chain	3-D	$S_{BET}=1957.3$ m^2/g (N$_2$ 77 K)	2018[10]
Ti$_3$-BPDC	**$Ti_3(BPDC)_3(OH)_2(OAc)_4$**	**Biphenyl-4,4'-dicarboxylate**	**3**	**3-D**	**$S_{BET}=636$ m^2/g (N$_2$ 77 K)**	**This work**

Note: Heterometallic Ti-MOFs reported in recent years are not included here.

2. Materials and Methods

All of the reactions and manipulations were carried out under N_2 with the use of a glovebox or Schlenk technique, unless otherwise indicated. Tetrahydrofuran and toluene were purified by passing through a neutral alumina column under N_2. Benzene, d_6-benzene, and *n*-octane were distilled over CaH_2. Pyridine and quinoline derivatives were purchased from Fisher or Aldrich, distilled, and then dried over 4Å molecular sieves prior to use. Pinacolborane was purchased from Sigma-Aldrich and distilled before use. Powder X-ray diffraction (PXRD) data was collected on Bruker D8 Venture diffractometer using Cu Kα radiation source (l = 1.54178 Å). N_2 sorption experiments were performed on a Micrometrics TriStar II 3020 instrument. Thermogravimetric analysis (TGA) was performed in air using a Shimazu TGA-50 equipped with a platinum pan and heated at a rate of 1.5 $^\circ$C per min. Fourier-transform infrared (FT-IR) spectra were collected using a Nexus 870 spectrometer (Thermo Nicolet) installed with Diffuse Reflectance Infrared Fourier Transform Spectroscopy (DRIFTS) system. X-ray Fluorescence (XRF) data was collected using a Rigaku NEX DE Energy Dispersive X-ray Fluorescence Spectrometer. X-ray photoelectron spectroscopy (XPS) data was collected using an AXIS Nova spectrometer (Kratos Analytical) with monochromatic Al Kα X-ray source; Al anode was powered at 10 mA and 15 kV, and the instrument work function was calibrated to give an Au $4f_{7/2}$ metallic gold binding energy (BE) of 83.95 eV. Instrument base pressure was ca. 1×10^{-9} Torr. The analysis area size was 0.3×0.7 mm^2. For calibration purposes, the binding energies were referenced to the C 1s peak at 284.8 eV. Survey spectra were collected with a step size of 1 eV and 160 eV pass energy. ICP-MS data was obtained with an Agilent 7700x ICP-MS and analyzed using ICP-MS MassHunter version B01.03. Samples were diluted in a 2% HNO_3 matrix and analyzed with a ^{159}Tb internal standard against a 12-point standard curve over the range from 0.1 ppb to 500 ppb. The correlation was >0.9997 for all analyses of interest. Data collection was performed in Spectrum Mode with five replicates per sample and 100 sweeps per replicate.

^{1}H NMR spectra were recorded on a Bruker NMR 500 DRX spectrometer at 500 MHz, and referenced to the proton resonance resulting from incomplete deuteration of $CDCl_3$ (δ 7.26) or C_6D_6 (δ 7.16). The following abbreviations are used herein: s: singlet, d: doublet, t: triplet, q: quartet, m: multiplet, br: broad, app: apparent. The conversions of reactions were determined by gas chromatography-mass spectrometry (GC-MS) using a Shimadzu GCMS-QP2010 Ulta equipped with SH-Rxi-5Sil MS 30 m × 0.5 mm × 0.25 µm column.

3. Synthesis and Characterization of Ti$_3$-BPDC

3.1 Synthesis of Ti$_6$O$_6$(O^{i}Pr)$_6$(abz)$_6$ cluster

The Ti$_6$O$_6$(O^{i}Pr)$_6$(abz)$_6$ (Habz = 4-aminobenzoic acid) cluster was synthesized according to a reported procedure.[11] To a 2-proponol solution (6.0 mL) containing 4-aminobenzoic acid (192.1 mg, 1.40 mmol) added was titanium(IV) isopropoxide (103.6 µL). After stirring for 30 min at room temperature, the orange slurry was heated at 100 °C for 77 h inside a sealed glass tube. The bright yellow crystalline product was collected, washed with 2-proponol and dried under vacuum for 3 h.

3.2 Synthesis of Ti$_3$-BPDC

Ti$_6$O$_6$(O^{i}Pr)$_6$(abz)$_6$ cluster (1 mg), biphenyl-4,4$^{'}$-dicarboxylic acid (3.74 mg), glacial acetic acid (15 uL), and DMF (1 mL) were charged in a 4 mL Pyrex vial. The mixture was heated in a 120 °C oven for 3 days. After cooling to room temperature, colorless transparent, rhombic crystals of the formula Ti$_3$(BPDC)$_3$(OH)$_2$(CH$_3$COO)$_4$ (Ti$_3$-BPDC) were harvested (0.5 mg, 31% yield). The powder X-ray diffraction (PXRD) pattern of the obtained MOF was compared to that of a simulated pattern based on the single-crystal structure to show the crystallinity and phase purity of the Ti$_3$-BPDC. No obvious TiO$_2$ peaks were observed based on our PXRD pattern (Figure 1b) for Ti$_3$-BPDC-syn, as well as the Ti$_3$-BPDC-CoCl and Ti$_3$-BPDC-CoH.[12, 13]

3.3 Single Crystal X-ray Crystallography of Ti$_3$-BPDC

The structure of Ti$_3$-BPDC was determnined by single crystal X-ray diffraction. The single crystal intensity data was collected at 298K on a Bruker D8 VENTURE with PHOTON 100 CMOS detector system equipped with a Mo-targeted micro-focus X-ray tube (λ= 0.71073 Å). Data reduction and integration were performed with the Bruker APEX3 software package (Bruker AXS, version 2015.5-2, 2015). Data were scaled and corrected for absorption effects using the multi-scan procedure as implemented in SADABS (Bruker AXS, version 2014/5, 2015, part of Bruker APEX3 software package). The structure was solved by SHELXT (Version 2014/5) and refined bu a full-matrix least-sqaures procedure using OLEX2 software package (XL refinement program version 2014/7). Crysallographic data and details of the data collection and structure refinement are listed in Table S2.
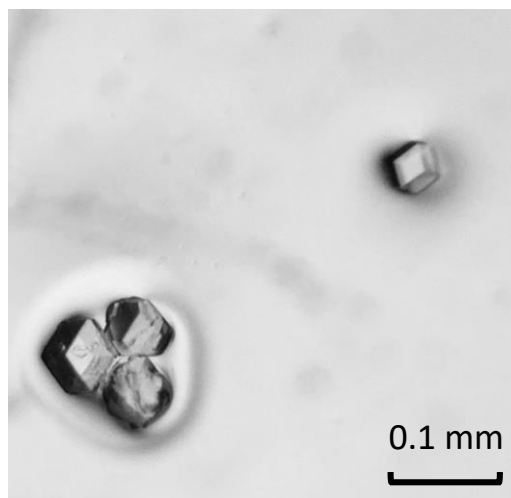
Figure S1. Optical microscope photo of Ti$_3$-BPDC single crystals used for X-ray structure determination.

Table S2. Crystallographic Information of Ti₃-BPDC.

Name	Ti₃-BPDC
CCDC	1859034
Formula	$C_{42}H_{26}O_{14}Ti_3$
Formula weight	898.26
Crystal system	Trigonal
Space group	$R\bar{3}m$
a, Å	25.8366(16)
b, Å	25.8366(16)
c, Å	13.6675(9)
α, deg	90
β, deg	90
γ, deg	120
V, Å³	7901.1(11)
Z	3
Temperature, K	296.96
F(000)	1380.0
Density (calcd. g/cm³)	0.569
Wavelegth, Å	0.71073
Absorption coeff. (mm⁻¹)	0.248
2Θ range data collection	4.706 to 49.454
Index ranges	$-30 \leq h \leq 30$ $-30 \leq k \leq 27$ $-16 \leq l \leq 15$
Reflections collected	16826
Indepedend reflections	1614
R(int)	0.0293
Data/restraints/parameters	1614/7/64
Goodness-of-fit on F²	1.607
Final R indices [I>2σ(I)]	

R indices (all data)	$R_1 = 0.1129$, $wR_2 = 0.3430$
	$R_1 = 0.1213$, $wR_2 = 0.3547$

100 Å
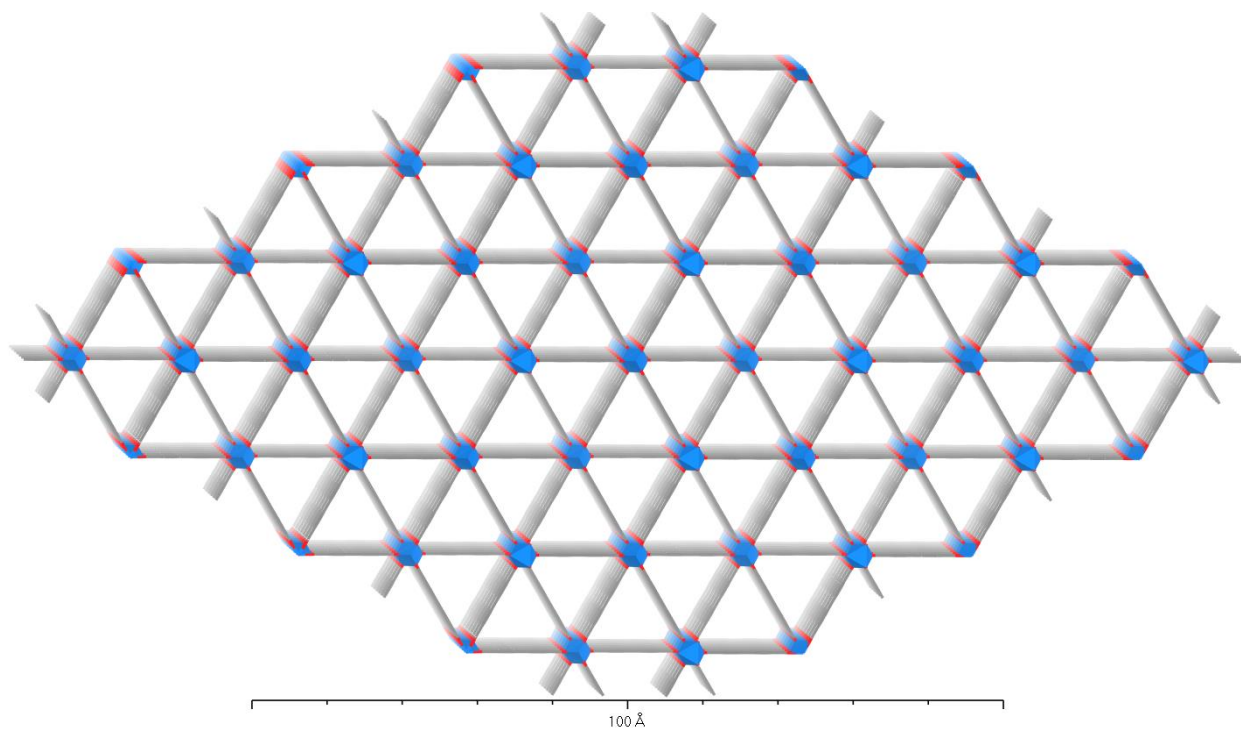
Figure S2. Crystal structure of Ti$_3$-BPDC as viewed along the c axis (H atoms omitted for clarity.

100 Å
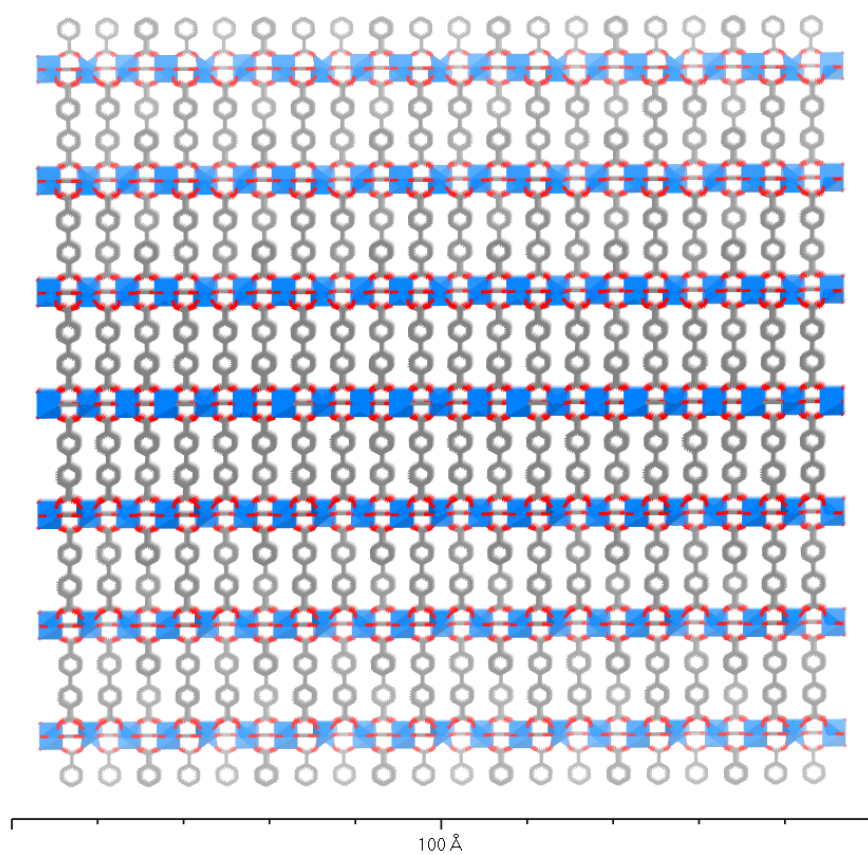
Figure S3. Crystal structure of Ti$_3$-BPDC as viewed along the *a* axis (H atoms omitted for clarity).

100 Å
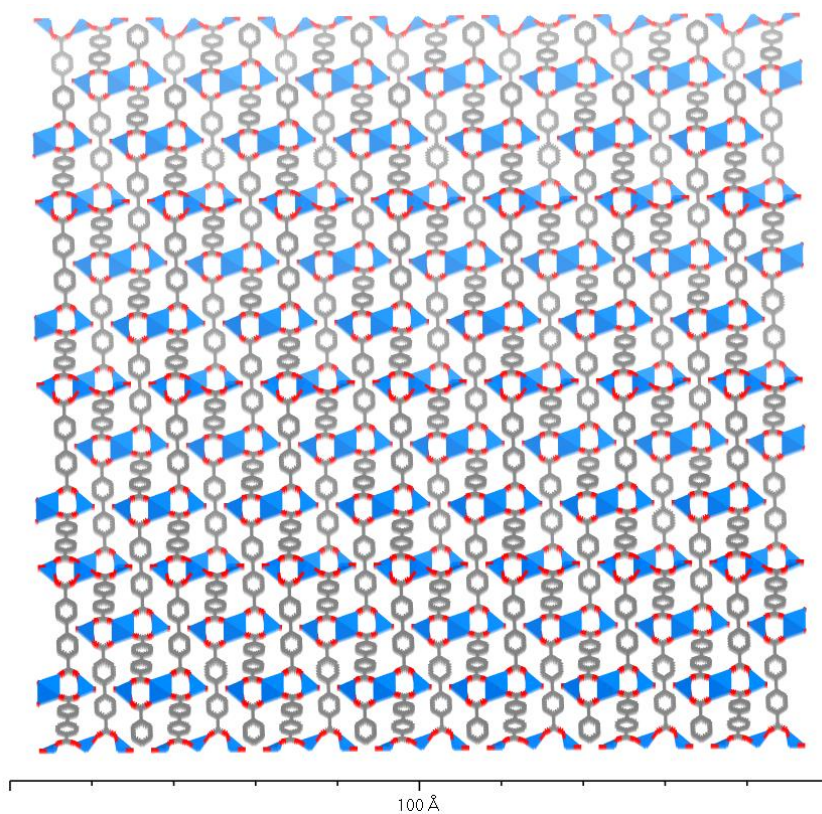
Figure S4. Crystal structure of Ti$_3$-BPDC as viewed along the *b* axis (H atoms omitted for clarity)

3.4 Topological Analysis of Ti$_3$-BPDC

The topological analysis of Ti$_3$-BPDC was performed using TOPOS 4.0 professional. The Ti$_3$ cluster is connected by six carboxylate groups. The overall structure is simplified into a unimodal 4-connected net with a point symbol of $\{6^6\}$, with the extended point symbol [6(2).6(2).6(2).6(2).6(2).6(2)].
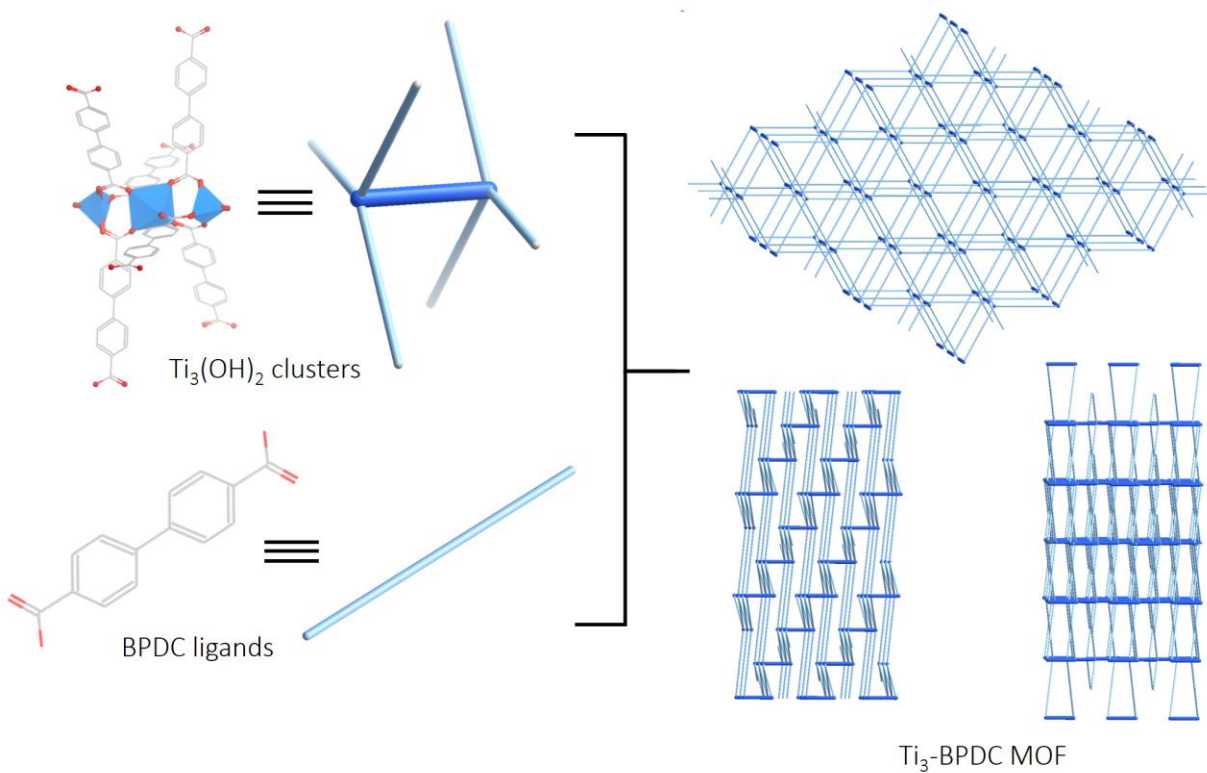
Figure S5. Schemetic representation of the 3D network of Ti$_3$-BPDC. Ti$_3$-BPDC has *dia* topology.

3.5 ^{1}H NMR spectra of digested Ti$_3$-BPDC

A dried sample of Ti$_3$-BPDC (1.0 mg) was digested by 100 uL D$_3$PO$_4$ (D, 99%), 50 uL HF (48%), and 50 uL D$_2$O. The sample was then sonicated for 3 h to completely dissolve Ti$_3$-BPDC, followed by adding 500 uL DMSO-d_6 for ^{1}H NMR analysis.
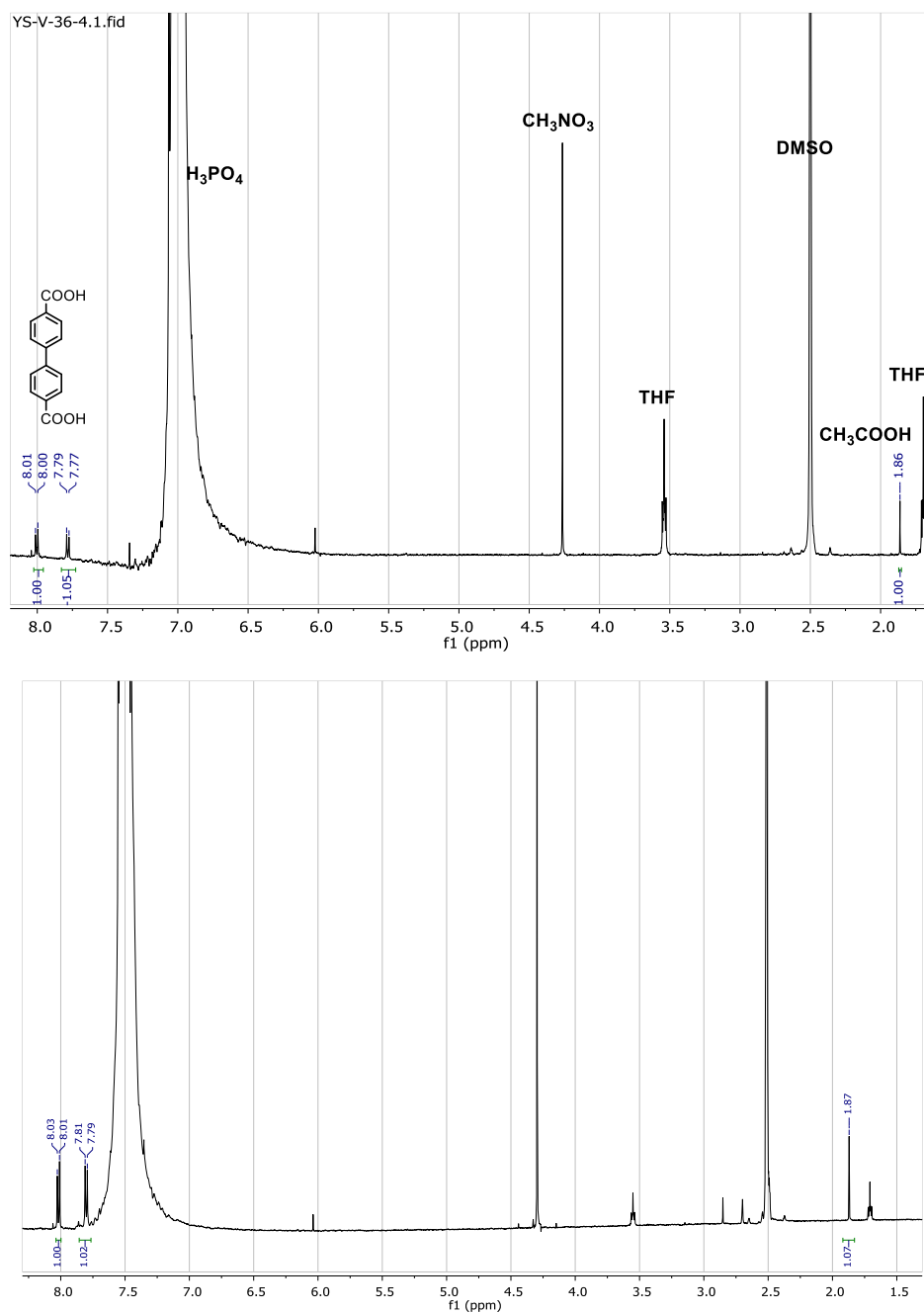
Figure S6. ^{1}H NMR spectra of digested Ti$_3$-BPDC. Based on the NMR data, we propose acetate as the counter anion in Ti$_3$-BPDC. Two parallel MOF digestion experiments were conducted. The ^{1}H NMR (500 MHz, DMSO-d_6) integral gave an average of 1.38 equiv. of acetates per BPDC ligand, corresponding well to the chemical formula Ti$_3$(BPDC)$_3$(OH)$_2$(CH$_3$COO)$_4$. CH$_3$NO$_2$ was added as an internal standard whereas THF was in the MOF channels.

3.6 Thermogravimetric Analysis
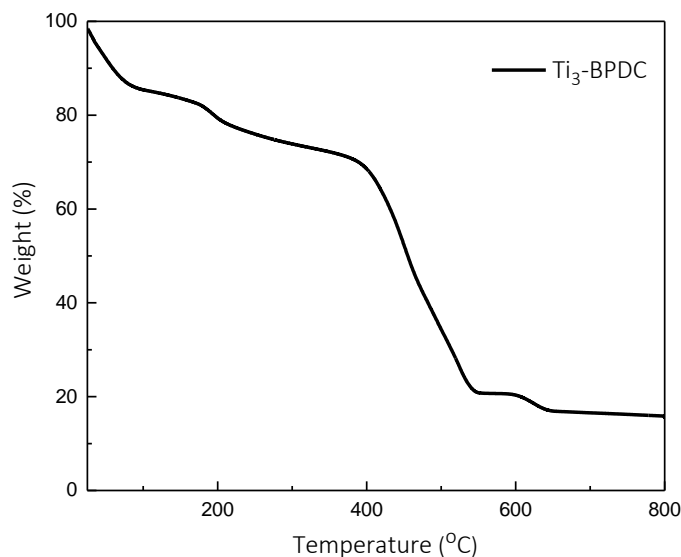
Figure S7. TGA curve of Ti$_3$-BPDC. The first weight loss (25.2%) in the 25-274 $^{\circ}$C temperature range corresponds to the removal of adsorbed solvents in the pores. The second weight loss (78.5%) in the 274-800 $^{\circ}$C temperature range corresponds to the decomposition of the MOF to TiO$_2$, consistent with the calculated weight loss of 78.9% based on the conversion from Ti$_3$(BPDC)$_3$(OH)$_2$(CH$_3$COO)$_4$ to (TiO$_2$)$_3$.

3.7 Nitrogen Sorption Isotherms of Ti$_3$-BPDC
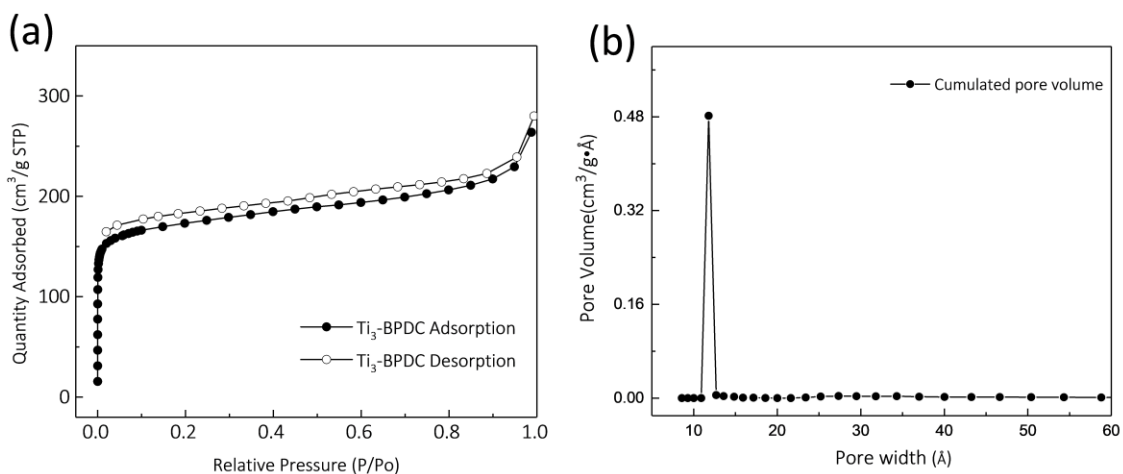
Figure S8. (a) Nitrogen sorption isotherms of Ti_3-BPDC (77K). Ti_3-BPDC has an BET surface areas of 636 m^2/g. **(b)** Pore size distributions of Ti_3-BPDC.

Theoretical surface area of Ti_3-BPDC was calculated to be 929 m^2/g using the Materials Studio software, which is slightly higher than the experimental surface area of 636 m^2/g. This discrepancy is possibly due to the presence of defects in the MOF structure and incomplete activation of the MOF before N_2 sorption studies.

y=4.7E-3x + 1.7E-6
BET surface area = 929 m^2/g
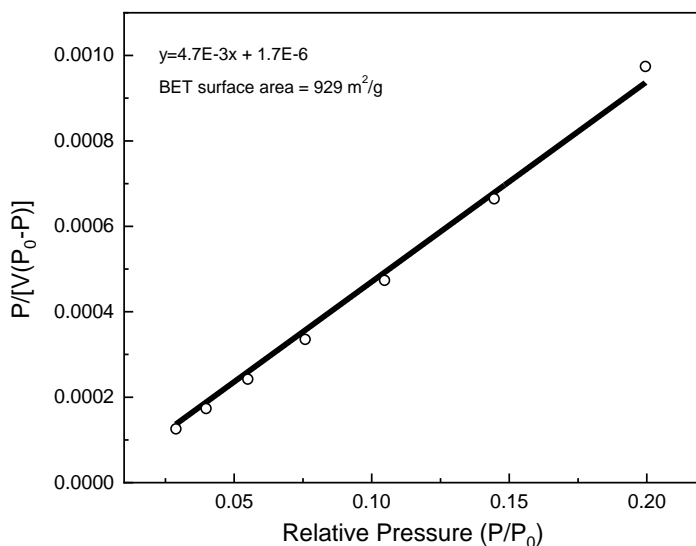
Figure S9. The BET Plot of the calculated N_2 isotherm of Ti_3-BPDC.

3.8 Isotope Labeling Experiment of Ti-OH in Ti₃-BPDC

1) $LiCH_2Si(CH_3)_3$

2) D_2O (3 eq)
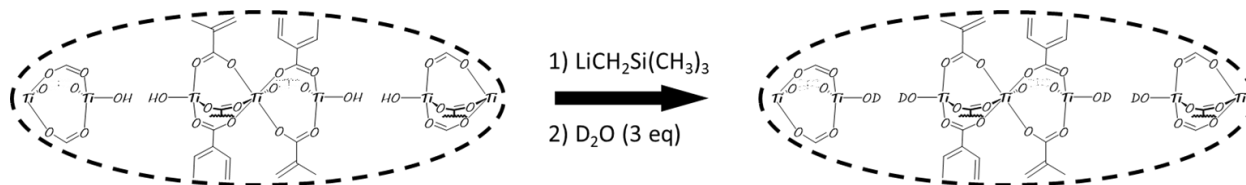
To further confirm the existence of Ti-OH groups in Ti_3-BPDC MOF, DRIFTS analysis was conducted on the isotopically labelled sample of Ti_3-BPDC. Specifically, Ti_3-BPDC was first fully deprotonated by 5 eq of $LiCH_2Si(CH_3)_3$ (*w.r.t.* Ti-OH) in hexanes. After removal of excess base, the deprotonated MOF was treated with 3 eq of D_2O to generate Ti_3-BPDC-OD. Ti_3-BPDC-

OD was evacuated at 50 °C for 24 h before DRIFTS analysis. Two main differences were observed between the IR spectra of Ti_3-BPDC-OH and Ti_3-BPDC-OD. First, the $\nu(Ti\text{-}\underline{OH}) = 3678$ cm^{-1} disappeared after H/D exchange, indicating the loss of Ti-OH groups. Second, two new stretching bands appeared at 2662 cm^{-1} and 2617 cm^{-1} in the DRIFTS spectra of Ti_3-BPDC-OD, which can be attributed to $\nu(Ti\text{-}\underline{OD})$ and $\nu(D_2O)$, respectively.[14, 15] The observed $\nu(Ti\text{-}\underline{OD})$ at 2662 cm^{-1} is in good agreement with the calculated $\nu(Ti\text{-}\underline{OD})$ of 2676 cm^{-1} based on reduced mass.
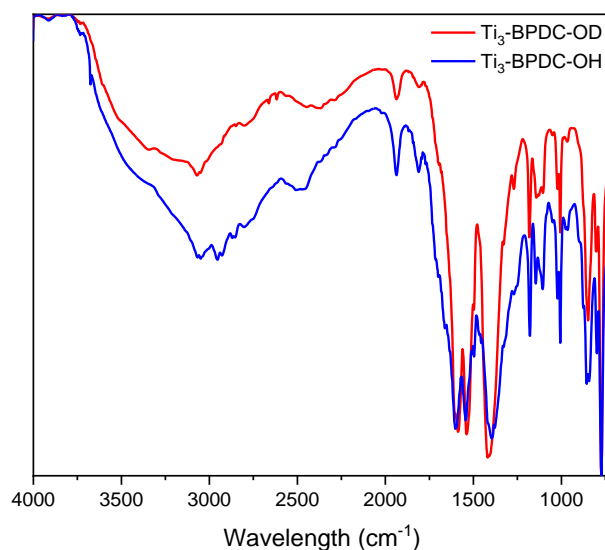
Figure S10. DRIFT spectra of Ti_3-BPDC-OH (=Ti_3-BPDC) and Ti_3-BPDC-OD (after H/D exchange).
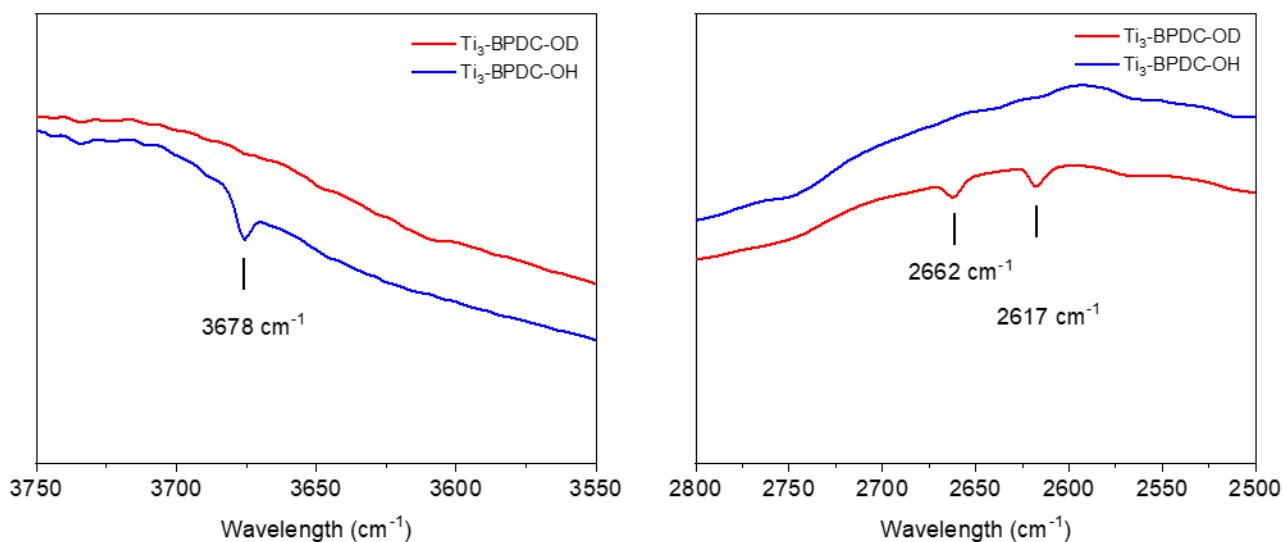
Figure S11. a) The disappearance of ν(Ti-<u>OH</u>) = 3678 cm^{-1} indicated the loss of Ti-OH groups. b) After H/D exchange, ν(Ti-<u>OD</u>) = 2662 cm^{-1} and ν(D$_2$O) = 2617 cm^{-1} were detected.

4. Synthesis and Characterization of Ti$_3$-BPDC-CoCl and Ti$_3$-BPDC-CoH

4.1 Synthesis of Ti$_3$-BPDC-CoCl

In a N$_2$-filled glovebox, Ti$_3$-BPDC (200 mg) in 15 mL THF was cooled to -30 °C for 30 min. To the cold suspension, LiCH$_2$SiMe$_3$ (1.0 M in pentane, 2 ml, 5 equiv. to μ-OH) was added dropwise and the resultant light yellow mixture was stirred at -30 °C for 3 h. The light yellow solid was collected after centrifugation, and washed with THF 5-6 times over 6 h. Then, the lithiated Ti$_3$-BPDC was transferred to a vial containing 20 mL THF solution of CoCl$_2$ (52 mg, 1 equiv. to μ-OLi). The mixture was stirred overnight and the deep blue solid was then centrifuged and washed with THF 5-8 times. The metalated MOF was stored in THF in the glovebox for further use. ICP-MS analysis indicated a Ti/Co ratio of 3.1. PXRD showed the crystallinity of MOF was maintained after metalation.

4.2 Single Crystal X-ray Crystallography of Ti$_3$-BPDC-CoCl
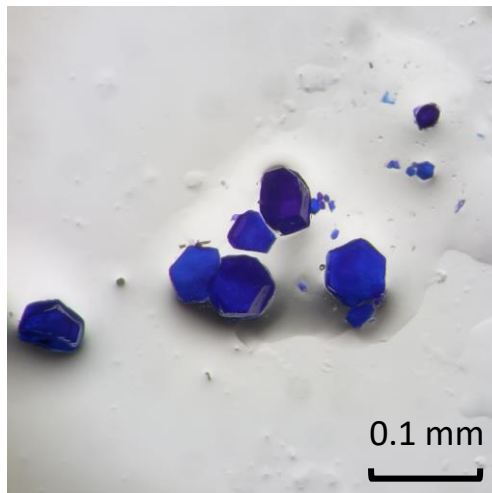
Figure S12. Optical microscope photo of typical Ti$_3$-BPDC-CoCl single crystals used for X-ray structure determination.

We made several attempts to obtain the single crystal structure of the metalated MOF. The Ti$_3$-BPDC-CoCl showed similar unit cell parameters and volume to the pristine MOF. However, due to the low resolution and highly disorder of Co centers, we failed to determine the single crystal structure after these trials.

Table S3. Crystallographic Information of Ti$_3$-BPDC-CoCl.

Name	Ti$_3$-BPDC-CoCl
a, Å	25.79
b, Å	25.79
c, Å	13.67
α, deg	90.00
β, deg	90.00
γ, deg	120.00
V, Å^3	7877
Temperature, K	296.96
Wavelegth, Å	0.71073

4.2 Thermogravimetric Analysis of Ti$_3$-BPDC-CoCl
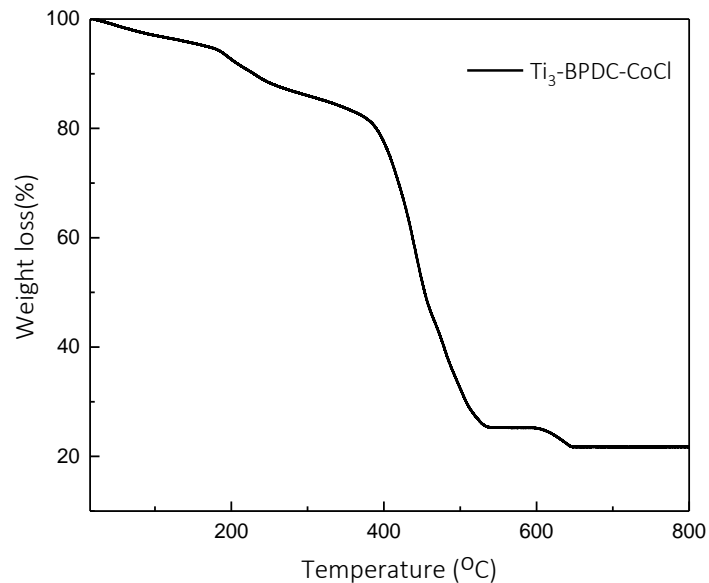
Figure S13. TGA curve of Ti$_3$-BPDC-CoCl. The first weight loss (14.5%) in the 25-312 °C temperature range corresponds to the removal of adsorbed solvents in the pores. The second weight loss (74.6%) in the 312-800 °C temperature range corresponds to the decomposition of the MOF to TiO$_2$, consistent with a calculated weight loss of 74.0% based on the conversion of Ti$_3$(BPDC)$_3$(O)$_2$CoCl(THF)Li(CH$_3$COO)$_4$ to (TiO$_2$)$_3$(Co$_2$O$_3$)$_{0.5}$(Li$_2$O)$_{0.5}$.

4.3 Nitrogen Sorption Isotherms of Ti$_3$-BPDC-CoCl
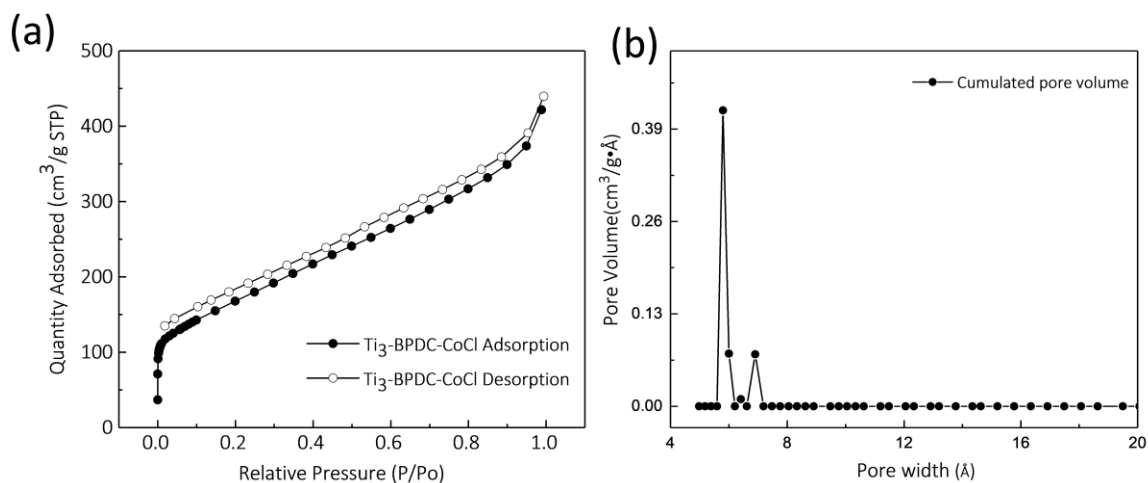
Figure S14. (a) Nitrogen sorption isotherms of Ti_3-BPDC-CoCl (77K). Ti_3-BPDC-CoCl has a BET surface areas of 480 m^2/g. **(b)** Pore size distributions of Ti_3-BPDC-CoCl.

4.4 MOF Structural Stability before and after Postsynthetic Metalation

To address the chemical stability of Ti_3-BPDC systems, a series of PXRD analyses were conducted on Ti_3-BPDC and Ti_3-BPDC-CoCl under different conditions (Figure S15). First, the PXRD patterns of the above two materials were checked after soaking in different solvents. Ti_3-BPDC and Ti_3-BPDC-CoCl were stable in both polar solvents, *e.g.*, DMF, THF, and non-polar solvent, *e.g.*, toluene. Then, MOF stability was examined by treatment with acid, base, and water in DMF. Ti_3-BPDC and Ti_3-BPDC-CoCl were stable in TEA/DMF (5:95, v/v). However, both Ti_3-BPDC and Ti_3-BPDC-CoCl lost their crystallinity when treated with water (H_2O/DMF, 5/95, v/v) or acid (HCl/DMF, 5/95, v/v). Furthermore, all of the above treatments and PXRD analyses were conducted in air, demonstrating MOF stability to oxygen and moisture in air.
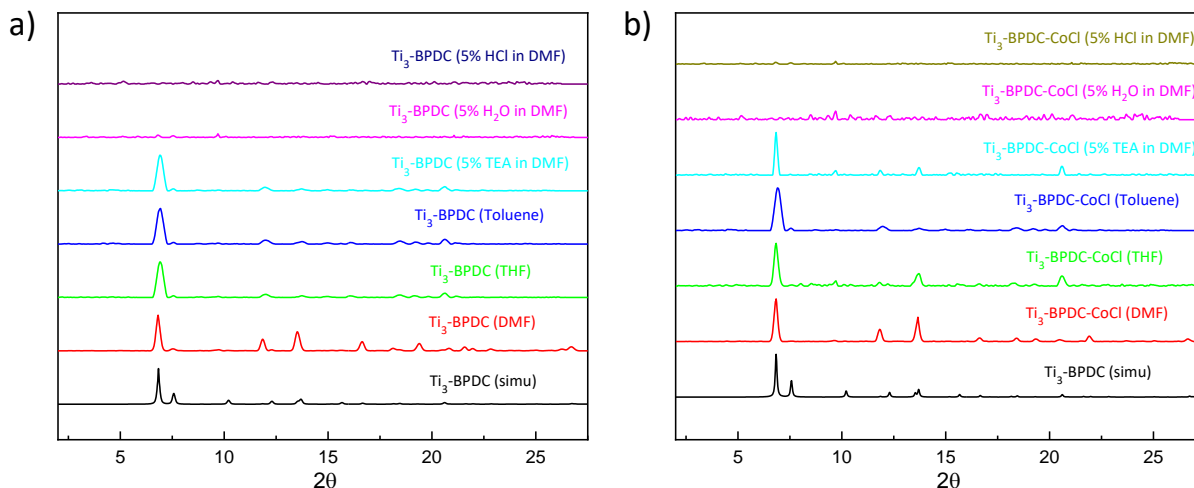
Figure S15. PXRD patterns of a) Ti_3-BPDC and b) Ti_3-BPDC-CoCl in different solvents and after treatment with acid, base, and H_2O.

4.5 Computational study on Ti_3-BPDC-CoCl

Density functional theory (DFT) calculations were performed for the Ti_3-BPDC-CoCl system using the Gaussian 09 software suite, version E01. These complexes were optimized in gas phase at the level of B3LYP/6-311G(d,p) theory. Charge distribuation was analyzed by natural population analysis (NPA).
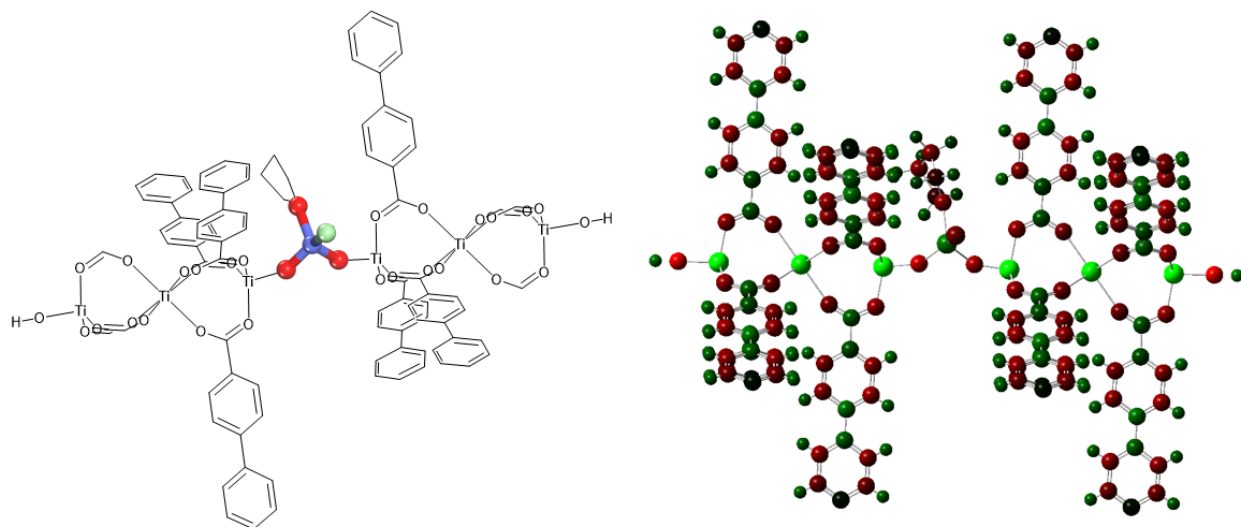
Figure S16. Optimized structure and calculated NBO charge distribution of the Ti_3-BPDC-CoCl fragment. Positively and negatively charged atoms are denoted by green and red colors, respectively.
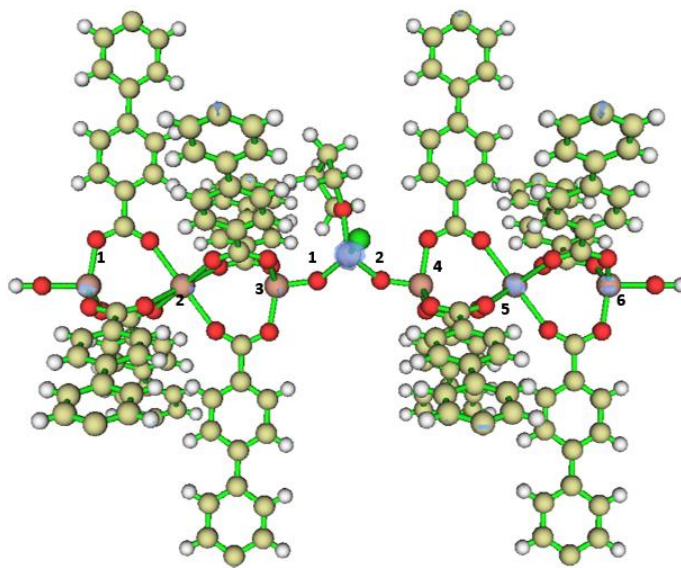
Figure S17. Spin density plot of the Ti$_3$-BPDC-CoCl fragment. The Co center have a spin density of 2.63.

Table S4: NBO charges and spin densities of selected fragment of Ti$_3$-BPDC-CoCl

	NBO Charge	Spin Density
Co	1.865827	2.634291
Cl	-0.96919	0.084018
Ti1	1.367511	0.249355
Ti2	0.9941	-0.01926
Ti3	1.399822	0.022101
Ti4	1.421932	0.018162
Ti5	1.001047	0.018605
Ti6	1.365814	-0.12666
O1	-0.92619	0.223447
O2	-0.79653	0.203426
O^{THF}	-0.67355	0.019917

4.6 EXAFS Fitting Using the DFT optimized Ti$_3$-BPDC-CoCl Structure

X-ray absorption data of Ti$_3$-BPDC-CoCl was collected at Beamline 10-BM at the Advanced Photon Source (APS) at Argonne National Laboratory. Spectra were collected at the cobalt K-edge (7709 eV) in transmission mode. The X-ray beam was monochromatized by a Si(111) monochromater and detuned by 50% to reduce the contribution of higher-order harmonics below the level of noise. A metallic cobalt foil standard was used as a reference for energy calibration and was measured simultaneously with experimental samples. The incident (I_0), transmitted (I_t), and reference (I_r) beam intensities were measured by 20 cm ionization chambers with gas compositions

of 63% N_2 and 37% He, 73% N_2 and 27% Ar, and 100% N_2, respectively. Data was collected over three regions: -200 to -20 eV (10 eV step size, integration time of 1.00 s), -20 to -50 eV (1 eV step size, integration time of 1.0 s), 50 eV to 14.98 Å^{-1} k (0.05 k step size, integration time of 1 s). Three X-ray absorption spectra were collected at room temperature for each sample. Samples were ground and mixed with polyethyleneglycol (PEG) and packed in a 6-shooter sample holder to achieve adequate absorption length.

Data was processed using the Athena and Artemis programs of the IFEFFIT package based on FEFF 6.[16, 17] Prior to merging, spectra were calibrated against the reference spectra and aligned to the first peak in the smoothed first derivative of the absorption spectrum, the background noise was removed, and the spectra were processed to obtain a normalized unit edge step. Fitting results are shown in Figure 1c. For fitting parameters, see Table S5.

Table S5. Summary of EXAFS fitting parameters for Ti$_3$-BPDC-CoCl

Ti$_3$-BPDC-CoCl		Fitting Range	k: 2.9 – 11.5 Å^{-1} R: 1 – 5 Å
Independent Points	13	**Variables**	7
Reduced chi-square	545	**R-factor**	0.015
ΔE$_0$(eV)	-9.36	**S$_0{}^2$**	1.05
R(Co-O$^{μ\text{-}OH1}$) (1)	1.89 ± 0.03 Å	**σ^2(Co-O$^{μ\text{-}OH1}$)**	0.004 ± 0.001
R(Co-O$^{μ\text{-}OH2}$) (1)	1.96 ± 0.03 Å	**σ^2 (Co-O$^{μ\text{-}OH2}$)**	0.004 ± 0.001
R(Co-O^{THF}) (1)	2.06 ± 0.03 Å	**σ^2 (Co-O^{THF})**	0.004 ± 0.001
R(Co-Cl) (1)	2.33 ± 0.08 Å	**σ^2 (Co-Cl)**	0.010 ± 0.005

4.7 Synthesis of Ti₃-BPDC-CoH

In a glovebox, Ti$_3$-BPDC-CoCl (5 μmol Co) in 1 mL toluene was dropwisely added NaBEt$_3$H (1.0 M in toluene, 0.05 ml, 10 equiv. to μ-OCoCl). The color of the suspension immediately changed from deep blue to black. After stirring at room temperature for 3 h, a black solid was collected after centrifugation and washed with toluene three times.
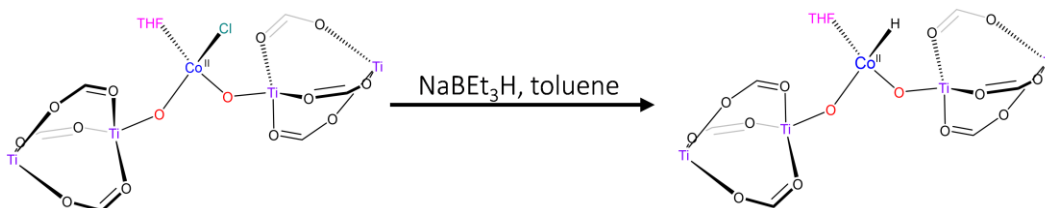
Figure S18. Conversion of Ti$_3$-BPDC-CoCl to Ti$_3$-BPDC-CoH.

4.8 X-ray Fluorosence Analysis before and after Cl/H Exchange

To provide further evidence for Cl/H exchange, X-ray fluorescence analysis was performed on Ti$_3$-BPDC-CoCl (before NaBEt$_3$H activation) and Ti$_3$-BPDC-CoH (after NaBEt$_3$H activation). As shown in Figure S19, the intensity of Cl in the MOF sample droped significantly after Cl/H exchange; 96.5% of Cl in the Ti$_3$-BPDC-CoCl sample had disappeared after NaBEt$_3$H activation and washing with solvents. The Co and Ti signals remained relatively unchanged before and after Cl/H exchange. X-ray fluorescence analysis thus showed that Co-Cl was nearly completely transformed into Co-H through Cl/H exchange after NaBEt$_3$H activation.
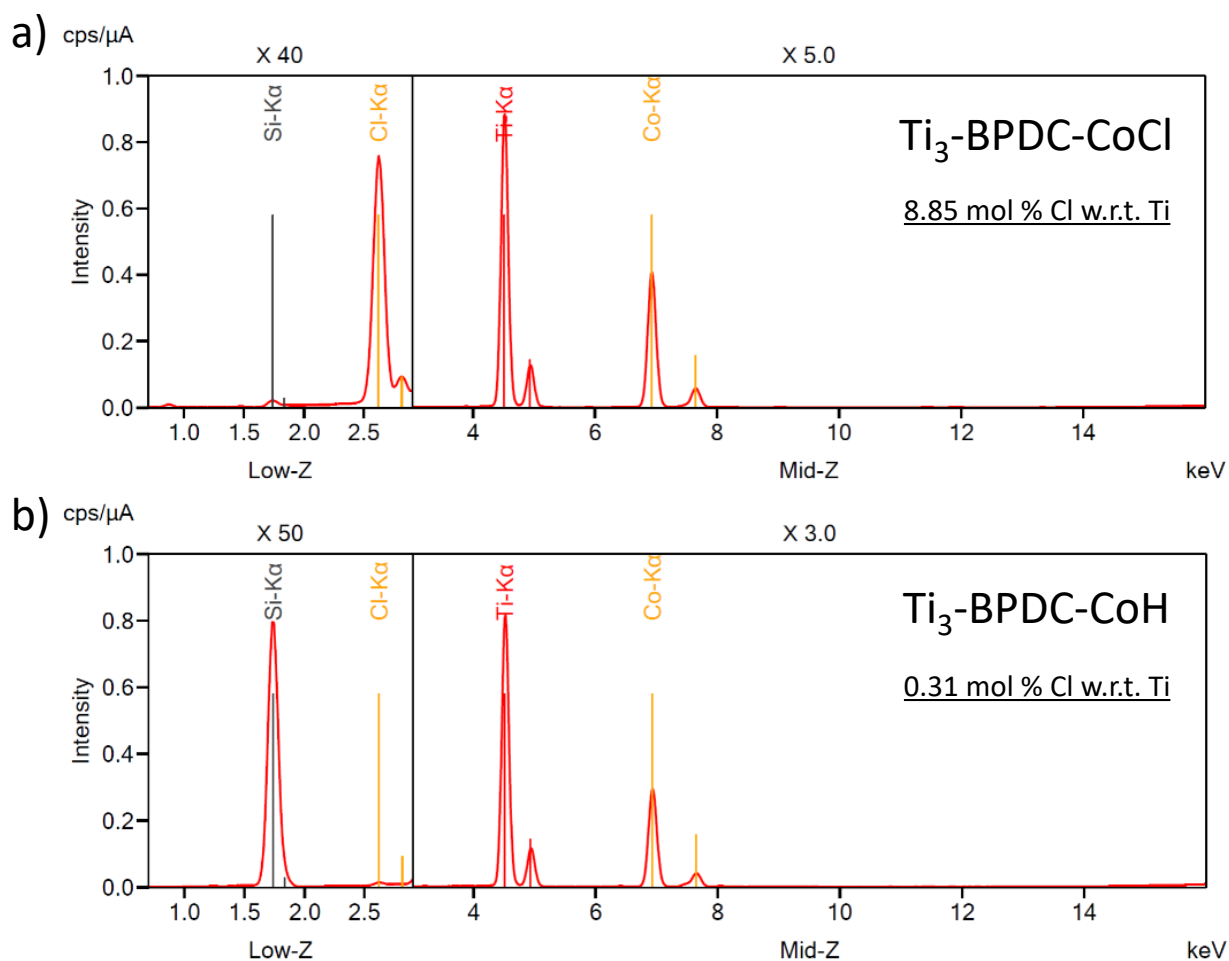
Figure S19. X-ray Fluoroscenece Spectra of a) Ti₃-BPDC-CoCl; b) Ti₃-BPDC-CoH.

4.9 Quantification of Hydrogen Prodcued from Protonation of Ti₃-BPDC-CoH

In a J. Young tube, Ti₃-BPDC-CoH (5 μmol of Co) in 1 mL toluene was treated with formic acid (0.9 μL, 50 μmol) and immediately sealed. After reacting at room temperature for 1 h, the head space gas was analyzed with GC to quantify the amount of H_2. Consistent results were obtained in three runs. The amount of H_2 was calculated to be 4.8 ± 0.21 μmol (expected 5 μmol).
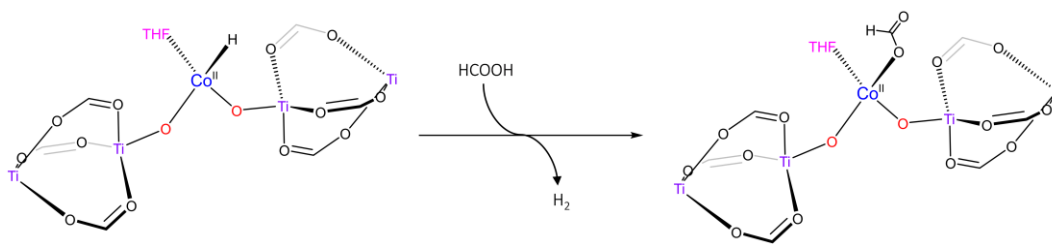
Figure S20. Hydrogen quantification of Ti$_3$-BPDC-CoH.
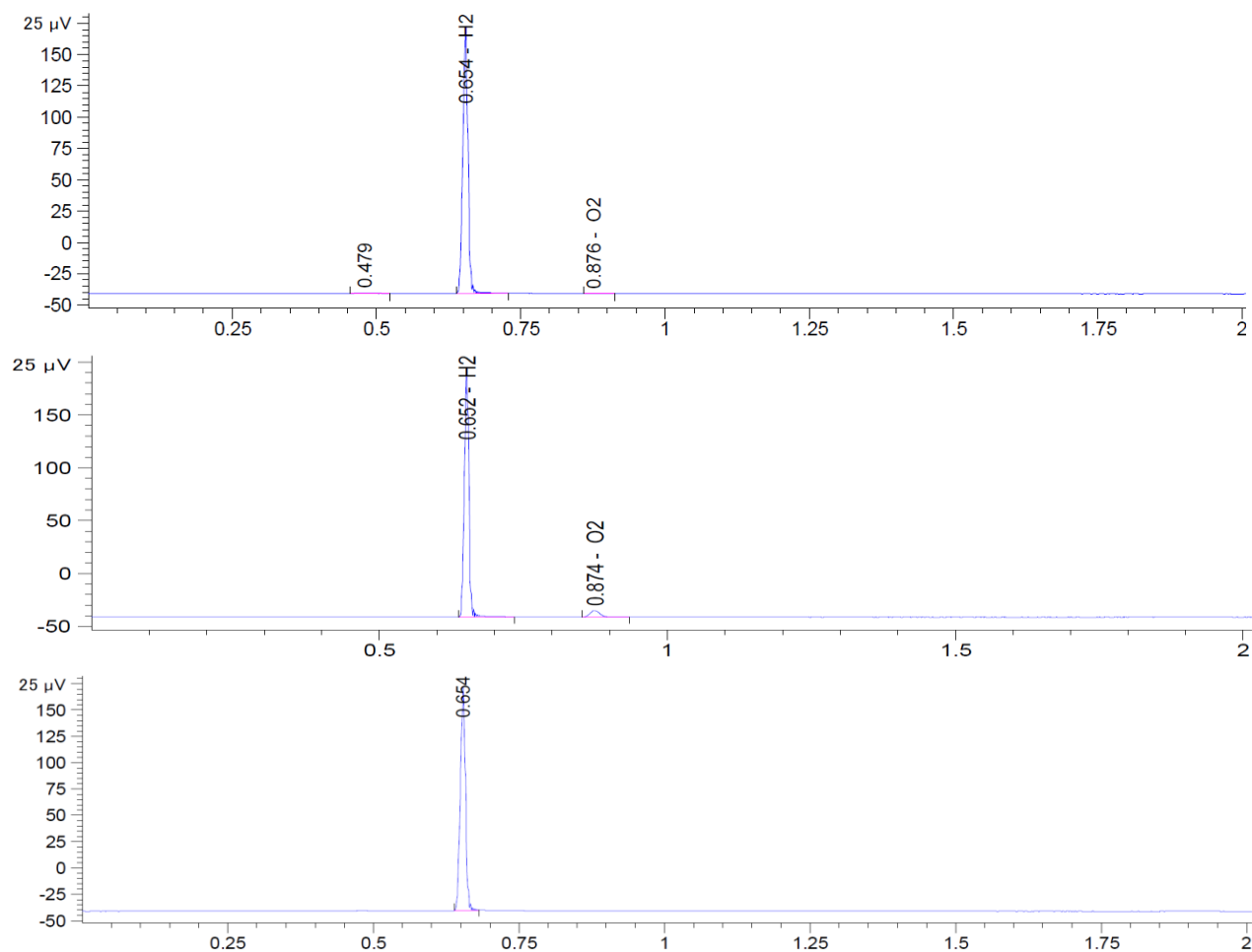
Figure S21. GC traces of H$_2$ evolved from protonation of Ti$_3$-BPDC-CoH with formic acid.

4.10 DFT Study on Ti$_3$-BPDC-CoH

DFT calculations were performed on the Ti_3-BPDC-CoH system using the Gaussian 09 software suite, version E01. These complexes were optimized in gas phase at the level of B3LYP/6-311G(d,p) theory. Charge distribuation was analyzed by natural population analysis (NPA).
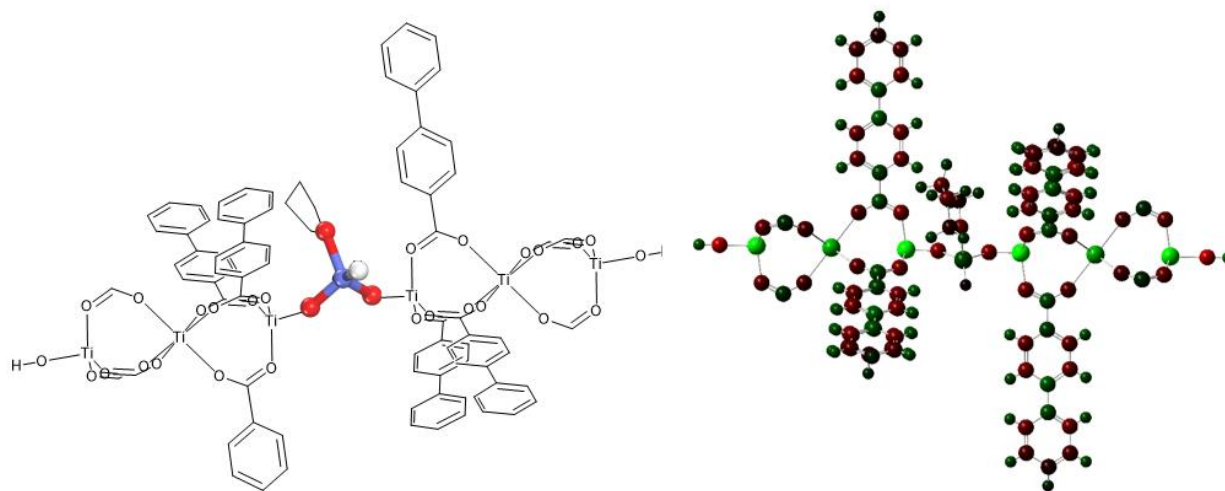
Figure S22. Optimized structure and calculated NBO charge distribution of the Ti_3-BPDC-CoH fragment. Positively and negatively charged atoms are denoted by green and red colors, respectively.
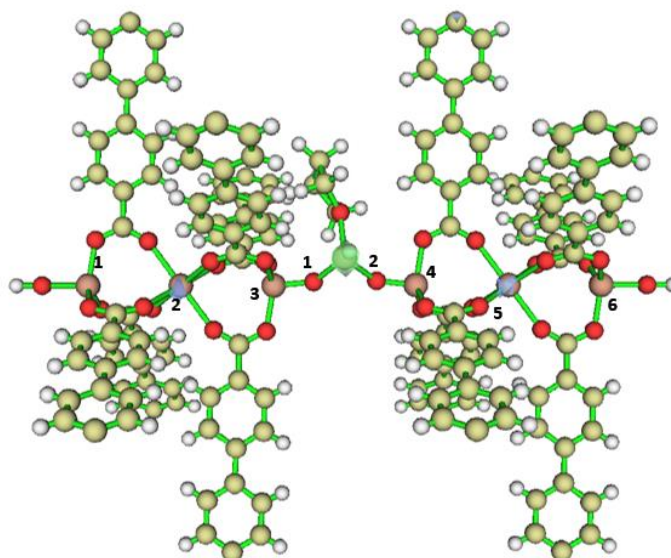
Figure S23. Spin density plot of the Ti_3-BPDC-CoH fragment. The Co center have a spin density of 2.71.

Table S6. NBO charges and spin density of selected fragment of Ti_3-BPDC-CoH

	NBO Charge	Spin Density
Co	1.524053	2.708781
H	-0.12265	0.109252
Ti1	1.364181	-0.853238
Ti2	0.992719	-1.893773
Ti3	1.355309	-0.452716
Ti4	1.389321	-0.098868
Ti5	0.996685	0.742935
Ti6	1.36406	-0.878587
O1	-0.94482	0.073799
O2	-0.91201	0.024723
O^{THF}	-0.85278	0.030206

4.11 EXAFS Fitting Using the DFT optimized Ti_3-BPDC-CoH Structure

X-ray absorption data of Ti_3-BPDC-CoH was collected and processed using identical protocol as Ti_3-BPDC-CoCl at 10-BM at Advanced Photon Source (APS) at Argonne National Laboratory. Fitting results are shown in Figure 2b. For fitting parameters, see Table S7.

Table S7. Summary of EXAFS fitting parameters for Ti_3-BPDC-CoH

Ti_3-BPDC-CoH		**Fitting Range**	k: 3 – 8.20 Å^{-1} R: 1.1 – 3.8 Å
Independent Points	9	**Variables**	6

Reduced chi-square	355	**R-factor**	0.008
ΔE_0(eV)	-3.06	**S_0^2**	1.05
R(Co-O$^{\mu\text{-OH1}}$) (1)	1.97 ± 0.04 Å	**σ^2(Co-O$^{\mu\text{-OH1}}$)**	0.004 ± 0.001
R(Co-O$^{\mu\text{-OH2}}$) (1)	2.00 ± 0.04 Å	**σ^2 (Co-O$^{\mu\text{-OH2}}$)**	0.004 ± 0.001
R(Co-O$^{\text{THF}}$) (1)	2.07 ± 0.04 Å	**σ^2 (Co-O$^{\text{THF}}$)**	0.004 ± 0.001
R(Co-H) (1)	1.61 ± 0.10 Å	**σ^2 (Co-H)**	0.002 ± 0.000

5. Ti$_3$-BPDC-CoH Catalyzed Cascade Reduction of Pyridines

5.1 Substrate Synthesis

5.1.1 3-Phenylpyridines derivatives
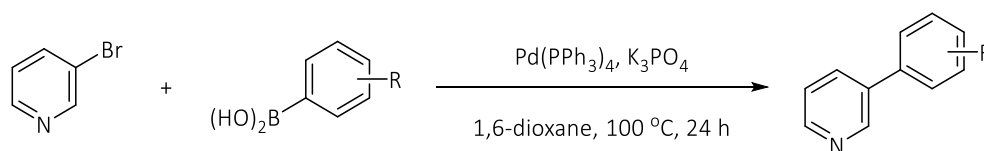
3-Phenylpyridines derivatives were synthesized by Suzuki coupling reactions. Phenylboronic acid with different substituents (6.0 mmol), tetrakis(triphenylphosphine)palladium(0) (289 mg, 0.25 mmol), and K$_3$PO$_4$ (3.18 g, 15 mmol) were charged into a dry round-bottom flask and dried under vacuum for 10 min. Degased 1,4-dioxane (30 mL) and 3-bromopyridine (0.48 mL, 790 mg, 5.0 mmol) were then added to the flask via a syringe. The mixture was stirred under N$_2$ at 100 °C for 24 h. After cooling to room temperature, the crude product was dispersed in 100 mL of H$_2$O, extracted with CH$_2$Cl$_2$ (30 mL × 4), and dried with Na$_2$SO$_4$. Pure 3-phenylpyridines were obtained after chromatography using hexane:ethyl acetate = 10:1(*v/v*) as elaunt. The ^{1}H NMR and ^{13}C NMR data of the products are consistent with those reported in literatures.

3-(p-tolyl)pyridine.[18] (CAS: 4423-09-0) White/pale yellow solid. Yield: 78%. ^{1}H NMR (500 MHz, Chloroform-d): δ 8.85 (dd, J = 2.4, 0.9 Hz, 1H), 8.57 (dd, J = 4.8, 1.6 Hz, 1H), 7.91 (ddd, J = 7.9, 2.4, 1.6 Hz, 1H), 7.51 – 7.47 (m, 2H), 7.39 (ddd, J = 7.9, 4.8, 0.9 Hz, 1H), 7.32 – 7.28 (m, 1H), 2.42 (s, 3H). ^{13}C NMR (126 MHz, Chloroform-d): δ 148.15, 148.12, 138.19, 136.79, 134.97, 134.36, 129.93, 127.09, 123.70, 21.28.
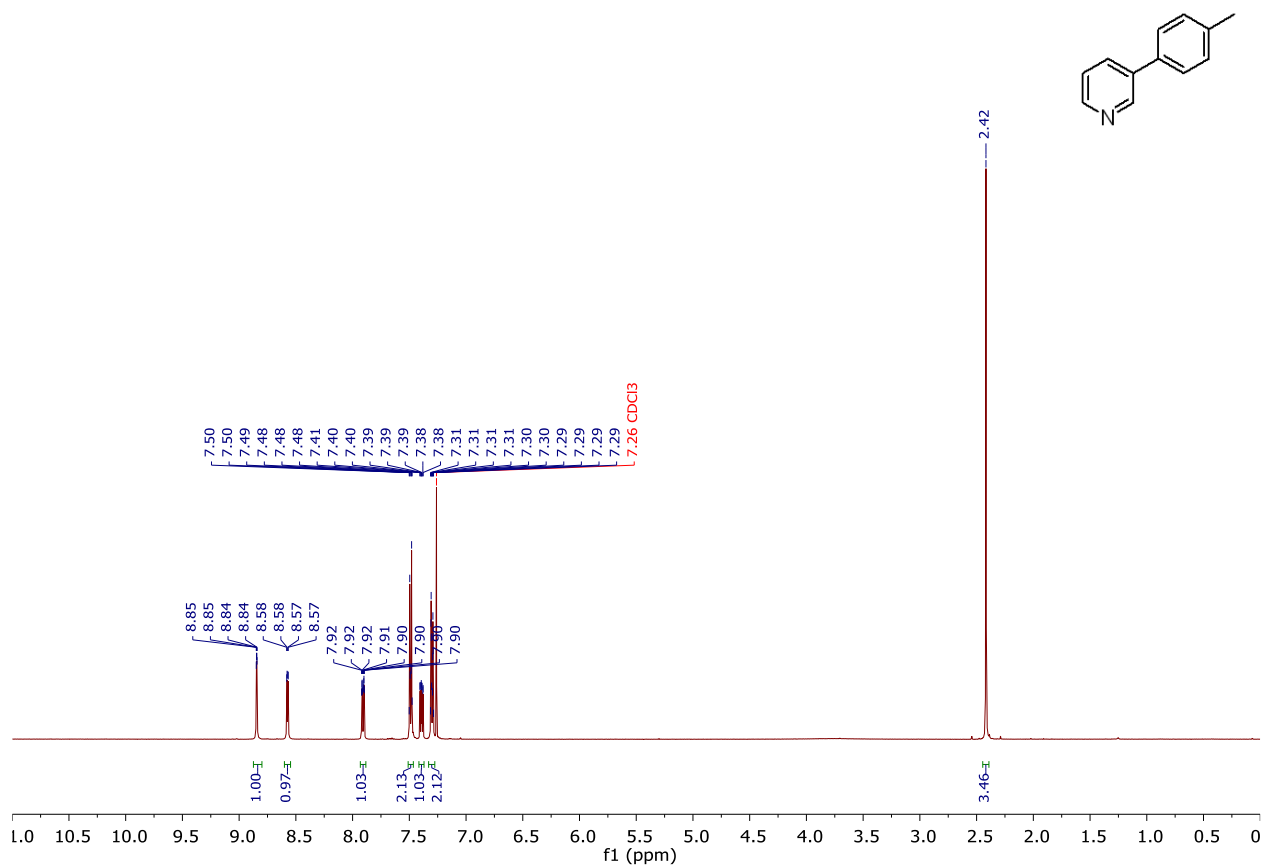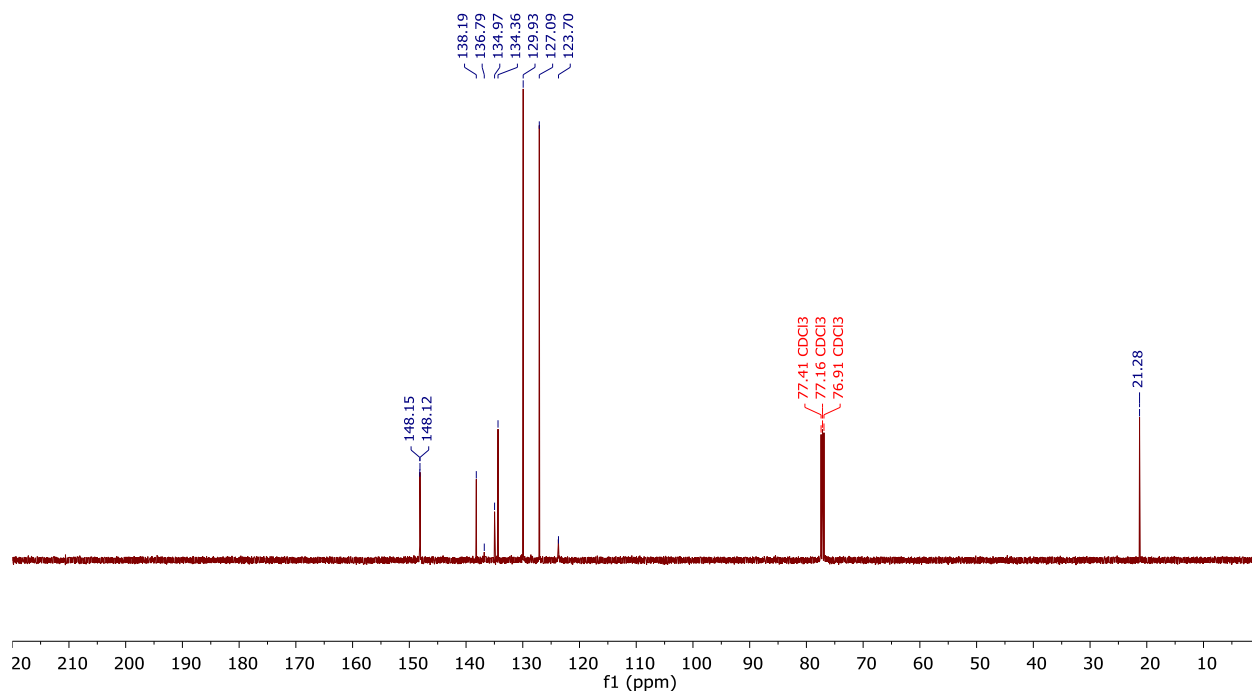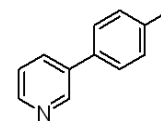
Figure S24. ^{1}H NMR and ^{13}C NMR spectrum of 3-(*p*-tolyl)pyridine.

3-(*m*-tolyl)pyridine.[18] (CAS: 4385-67-5) Colorless liquid. Yield: 90%. ^{1}H NMR (500 MHz, Chloroform-*d*): δ 8.85 (dd, *J* = 2.4, 0.9 Hz, 1H), 8.59 (dd, *J* = 4.8, 1.6 Hz, 1H), 7.90 (ddd, *J* = 7.9, 2.4, 1.6 Hz, 1H), 7.41 – 7.36 (m, 4H), 7.25 – 7.22 (m, 1H), 2.44 (s, 3H). ^{13}C NMR (126 MHz, Chloroform-*d*): δ 148.31, 138.90, 137.86, 136.98, 134.62, 129.11, 129.00, 128.03, 124.37, 123.70, 21.64.

7.40
7.40
7.40
7.39
7.39
7.39
7.38
7.38
7.38
7.37
7.26 CDCl3
7.25
7.24
7.24
7.24
7.24
7.23
7.23
7.23
7.22

8.85
8.85
8.85
8.84
8.60
8.59
8.59
8.58

7.92
7.91
7.91
7.91
7.90
7.90
7.89
7.89

2.44

1.00
0.96
0.99
3.98
0.94
3.28

f1 (ppm)

138.90
137.86
136.98
134.62
129.11
129.00
128.03
124.37
123.70

148.31

77.41 CDCl3
77.16 CDCl3
76.91 CDCl3

21.64

f1 (ppm)

S30
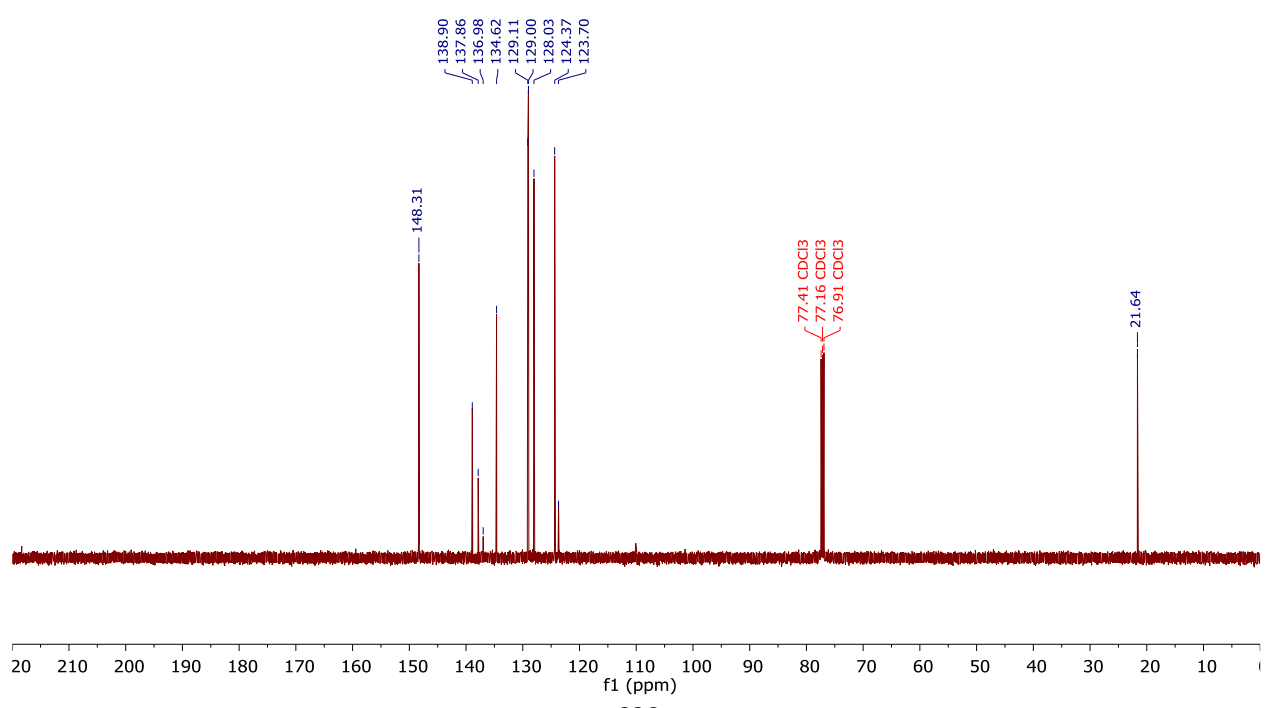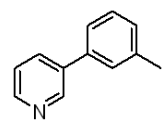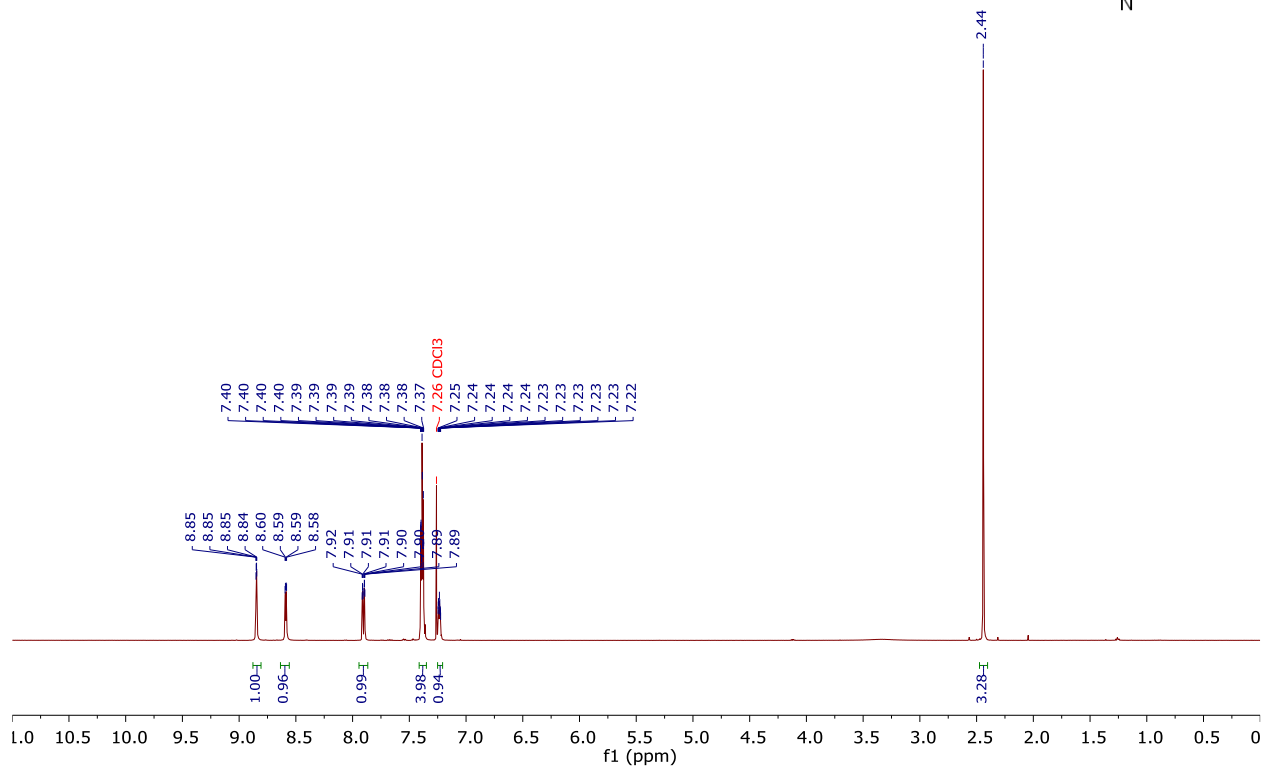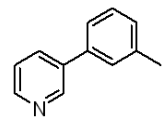
Figure S25. ^{1}H NMR and ^{13}C NMR spectrum of 3-(*m*-tolyl)pyridine.

3-(*o*-tolyl)pyridine.[19] (CAS: 90395-49-6) Colorless liquid. Yield: 93%. ^{1}H NMR (500 MHz, Chloroform-*d*): δ 8.65-8.58 (m, 2H), 7.74 (ddd, *J* = 7.8, 2.3, 1.7 Hz, 1H), 7.43 (ddd, *J* = 7.8, 5.0, 0.9 Hz, 1H), 7.35 – 7.27 (m, 3H), 7.22 (ddd, *J* = 7.2, 1.3 Hz, 1H), 2.28 (s, 3H). ^{13}C NMR (126 MHz, Chloroform-*d*): δ 149.72, 147.88, 138.04, 137.75, 136.96, 135.71, 130.73, 129.99, 128.33, 126.25, 123.27, 20.50.
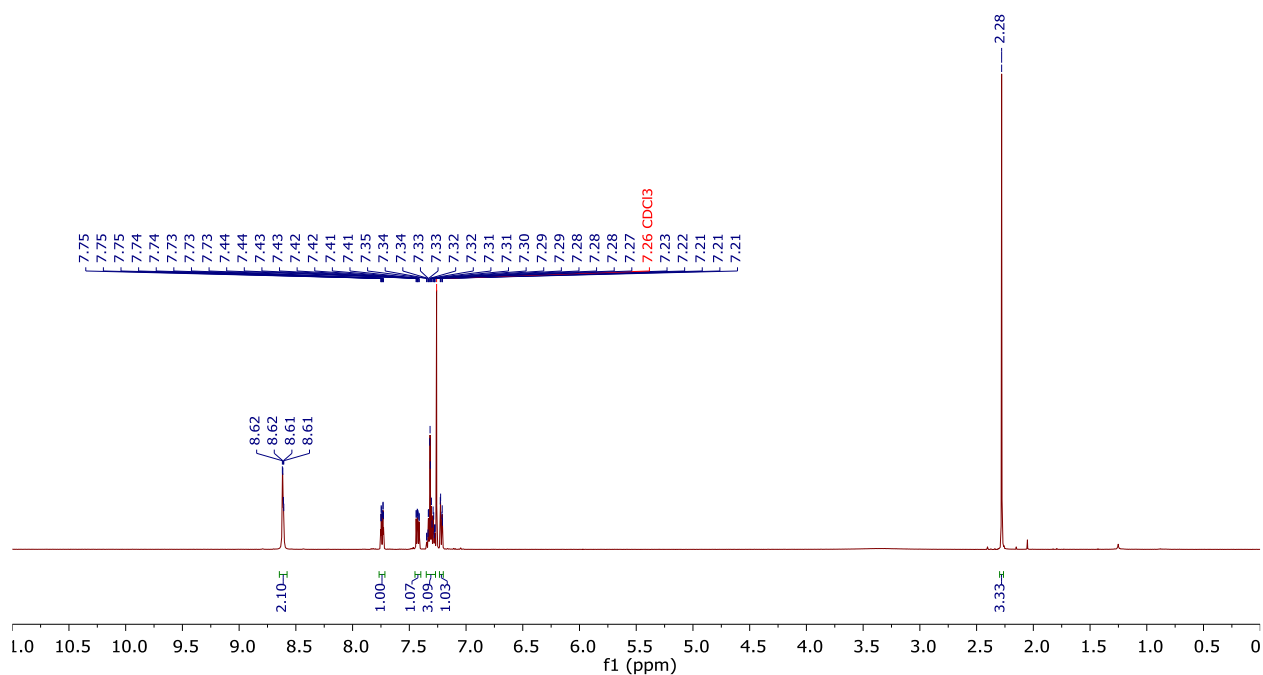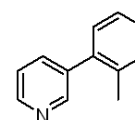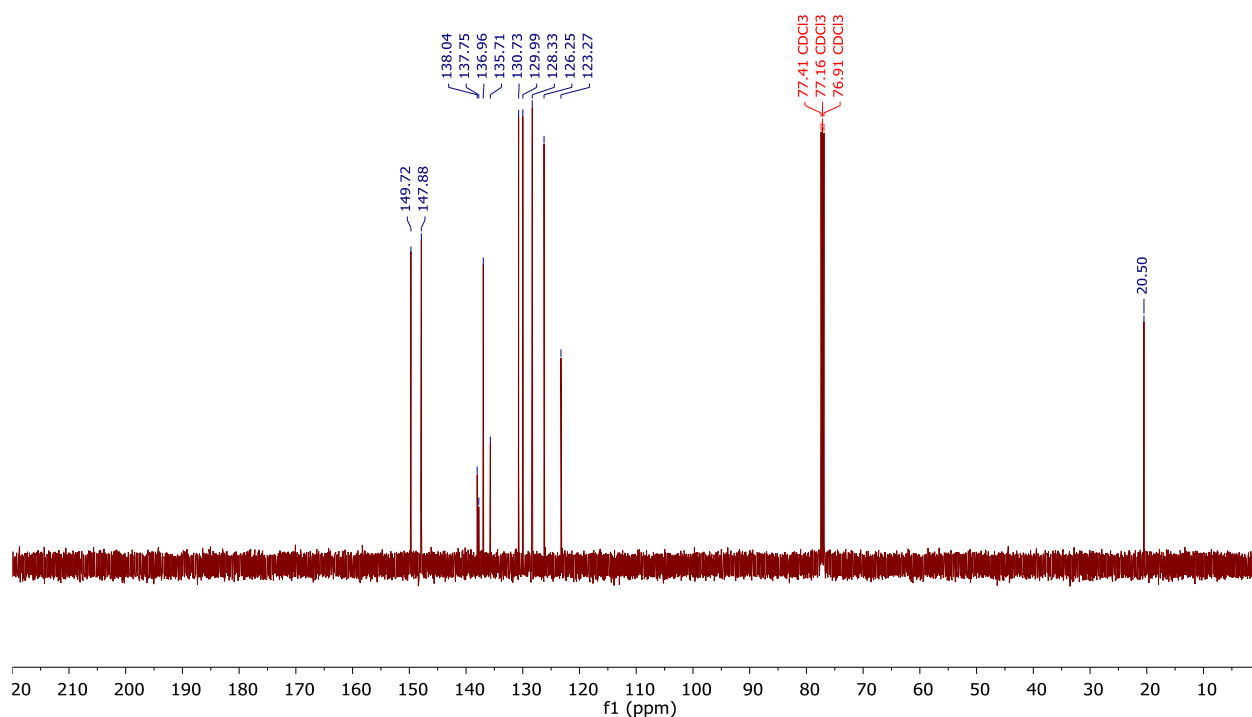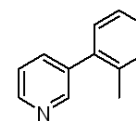
Figure S26. ^{1}H NMR and ^{13}C NMR spectrum of 3-(o-tolyl)pyridine.

5.1.2 1,2/1,4-Hydroboration adducts of pyridine and 6-methoxylquinoline
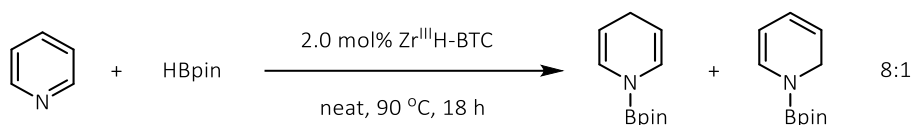
Zr[III]H-BTC (0.04 mmol Zr) was prepared according to the literature.[20] Pyridine (160 µL, 2.0 mmol) was then added to a mixture of Zr[III]H-BTC and pinacolborane (319 µL, 2.2 mmol). The reaction mixture was stirred under N_2 at 90 °C for 18 h. The MOF was removed from the solution by filteration. The supernatant was concentrated in vacuo to afford a mixture of 1-(4,4,5,5-tetramethyl-1,3,2-dioxaborolan-2-yl)-1,4-dihydropyridine (1,4-adduct, 1.78 mmol, 89% NMR yield based on mesitylene as an internal standard) and 1-(4,4,5,5-tetramethyl-1,3,2-dioxaborolan-

2-yl)-1,2-dihydropyridine (1,2-adduct, 0.22 mmol, 11% NMR yield based on mesitylene as an internal standard). The ^{1}H NMR peaks correspond well to the reported data.
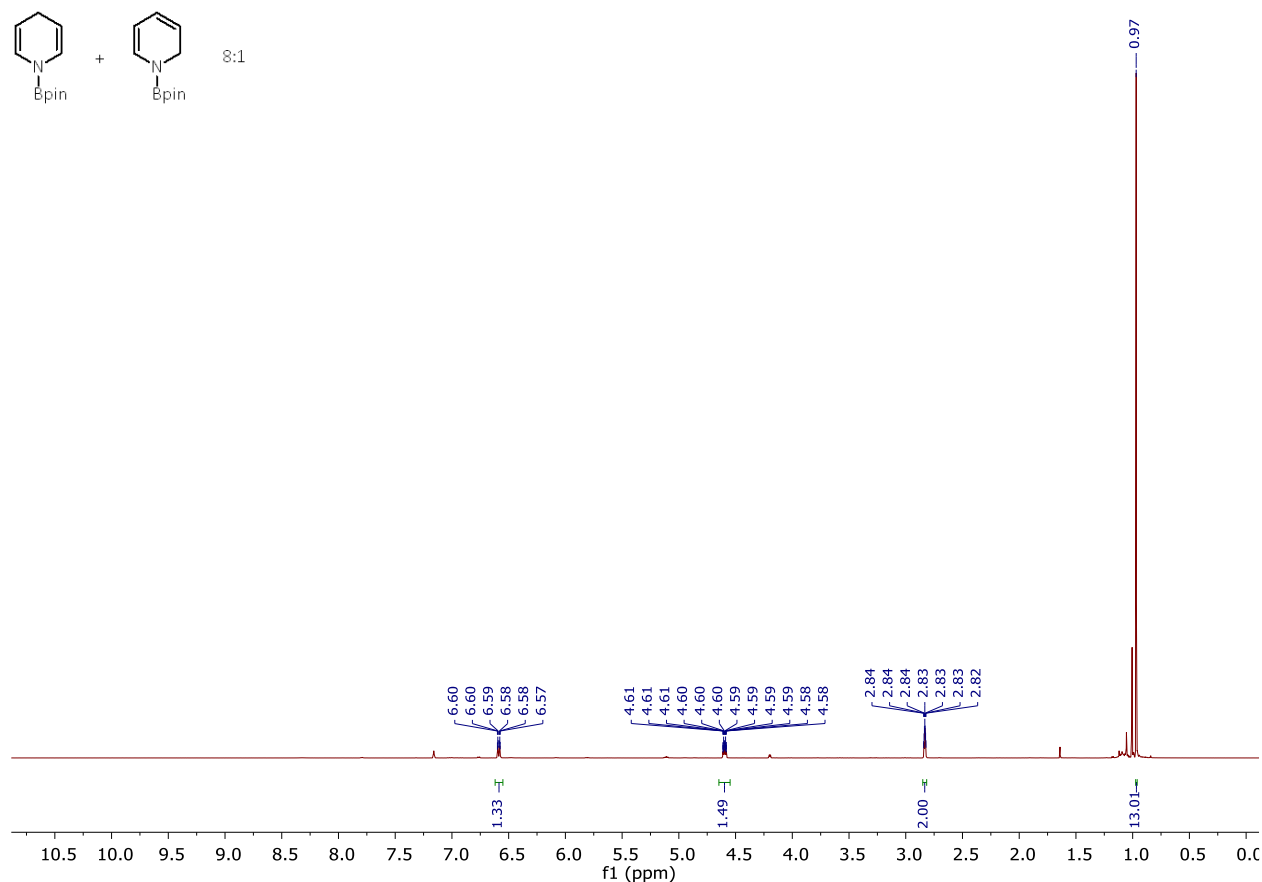
Figure S27. ^{1}H NMR spectrum of Zr^{III}-BTC catalyzed pyridine hydroboration product.
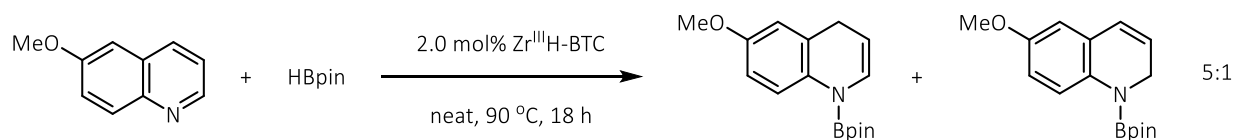
6-Methoxyquinoline (276 μL, 2.0 mmol) was added to a mixture of Zr^{III}H-BTC (0.04 mmol Zr) and pinacolborane (319 μL, 2.2 mmol). The reaction mixture was stirred under N$_2$ at 90 °C for 18 h. The MOF was removed from the solution by filteration. The supernatant was concentrated in vacuo to afford a mixture of 6-methoxy-1-(4,4,5,5-tetramethyl-1,3,2-dioxaborolan-2-yl)-1,4-dihydroquinoline (1,4-adduct, 1.67 mmol, 83% NMR yield based on mesitylene as an internal standard) and 6-methoxy-1-(4,4,5,5-tetramethyl-1,3,2-dioxaborolan-2-yl)-1,2-dihydroquinoline

(1,2-adduct, 0.33 mmol, 17% NMR yield based on mesitylene as an internal standard). The ^{1}H NMR peaks correspond well to the reported data.
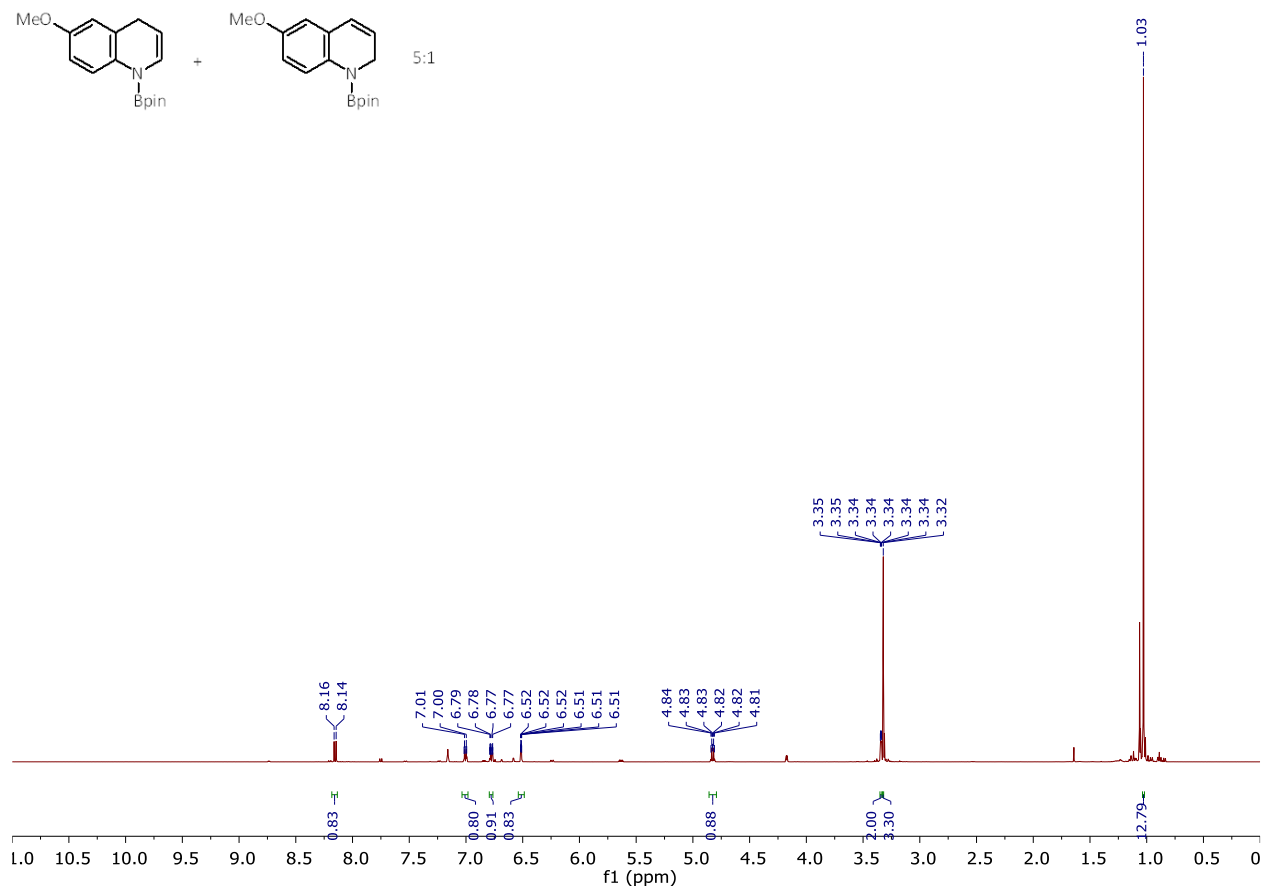
Figure S28. ^{1}H NMR spectrum of Zr^{III}-BTC catalyzed 6-methoxylquinoline hydroboration product.

5.2 Condition optimization and control experiments of Ti_3-BPDC-CoH catalyzed cascade reduction of pyridines.

Early trials of Ti_3-BPDC-CoH catalytzed cascade reduction of 3-picoline were conducted at 0.5% cat. Loading in 1 mL octane as solvent, with 3.00 equiv. of HBpin, 50 bar H_2 pressure, at 100 °C for 22 hrs. Over 99% of 3-methylpiperidine was detected by GC-MS using mesitylene as internal standard. Later experiments (Entry 2-6, Table S8) showed that 0.2% cat. loading, 1.05 equiv. of HBpin and 20 bar H_2 was required to achieve good yield (>95%). Dramatic yield drop was observed when the solvent was changed to either THF, Toluene, or neat condition (Entry

7,8,12, Table S8). Decrease the temperature to 80 °C afforded no product (Entry 9, Table S8). The maximum TON was achieved at 0.05 mol% catalyst loading for 3 days, with TON = 1980.

Table S8. Optimization of conditions for Ti_3-BPDC-CoH catalyzed cascade reduction using 3-picoline as substrate.[a]
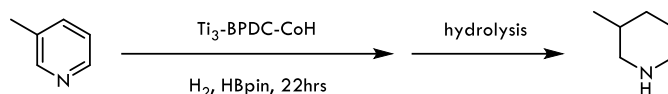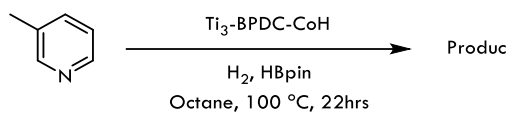
Entry	Cat. Loading / %	Solvent	HBpin equivalent	H_2 pressure / bar	Temp. / °C	Yield / %
1	0.5	Octane	3.00	50	100	>99
2	0.2	Octane	3.00	50	100	>99
3	0.2	Octane	1.05	20	100	97
4	0.2	Octane	0.30	50	100	26
5	0.05	Octane	1.05	20	100	65
6	0.05	Octane	1.05	5	100	2
7	0.2	THF	1.05	20	100	4
8	0.2	Toluene	1.05	20	100	10
9	0.2	Octane	1.05	20	80	0
10	0.2	Octane	1.05	20	120	>99
11[b]	0.05	Octane	1.05	20	100	99
12	0.01	neat	1.05	50	100	0
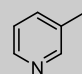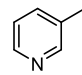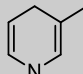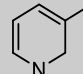
[a]Reaction conditions: Ti_3-BPDC-CoH (Loading w.r.t. Co), 0.5 mmol 3-picoline, 0 ~ 3.0 equiv. pinacolborane, 20 ~ 50 bar H_2, 1 mL Solvent; Yield was determined by GC-MS analysis, mesitylene as internal standard. [b]Reaction time: 3 days.

Background reactions and HBpin/H_2 control experiments were conducted for the Ti_3-BPDC-CoH catalyzed cascade reduction. The reaction did not proceed in the absence of either Ti_3-BPDC-CoH MOF or HBpin, even when the H_2 pressure was increased to 50 bar (Entry 1-2, Table S9). In the absence of H_2, 1,4- and 1,2-hydroboration products were obtained, but the TON was significantly lower than that of the cascade reduction. At 2.0 mol% of Co loading with 1.5 equiv. of HBpin, 15% of 15% of 1,4-hydroborated 3-picoline and 10% of 1,2-hydroborated 3-picoline

were obtained in 22 hours based on ^{1}H NMR analysis (Entry 3, Table S9). These results indicate that the catalyst (Ti$_3$-BPDC-CoH), HBpin, and H$_2$ are essitial for the catalytic cascade process and the coupling of the hydrogenation step promotes the cascade reduction by pushing the equilibrium to the reduced product.

Table S9. Background reactions and HBpin/H$_2$ control experiments for Ti$_3$-BPDC-CoH catalyzed cascade reduction using 3-picoline as substrate.[a]

Entry	Cat. Loading / %	HBpin equivalent	H$_2$ pressure / bar	Product
1	0.5	0	50	>99% of 3-picoline recovered[a] >99%
2	0	3.00	50	>99% of 3-picoline recovered[a] >99%
3	2.0	1.50	0	15% of 1,4-hydroborated 3-picoline + 10% of 1,2-hydroborated 3-picoline[b] 15% 10%

[a]Yield was determined by GC-MS analysis, mesitylene as internal standard. [b]Yield was determined by ^{1}H NMR analysis, mesitylene as internal standard.

To further prove that the Co-hydride sites supported on the Ti$_3$-BPDC MOF act as the real catalytic species in the cascade reduction of pyridines, a series of control experiments were conducted using different catalysts (Table S10). First, Ti$_3$-BPDC-CoCl was used as catalyst without first being treated with NaBEt$_3$H. Under the same Co loading and reaction condiction, Ti$_3$-BPDC-CoCl showed no activity in the cascade reduction of 3-picoline. Second, to rule out the

possiblility of Ti sites in catalyzing the reaction, Ti$_3$-BPDC was used as the catalyst with the same amount of Ti amount in Ti$_3$-BPDC-CoH. No product was detected. Third, Co nanoparticles (NPs) were also applied in the cascade reduction. Co-NPs were obtained by treating CoCl$_2$/THF solution with 10 eq. of NaBEt$_3$H and washed with toluene three times and then added to the reactor. Co-NPs, at the same Co loading as Ti$_3$-BPDC-CoH, showed no catalytic activity, further ruling out the possibility of leached Co species responsible for the cascade reduction product. Finally, 2 mol% of NaBEt$_3$H was used as the catalyst but no product was obtained, excluding the possibility of trapped NaBEt$_3$H in the MOF channel catalyzing the cascade reaction. These experiments rule out the possibility of potential leaching process (leading to Ti$_3$-BPDC and Co-NPs) or the NaBEt$_3$H being responsible for the cascade reduction product.

Table S10. Control experiments using different catalysts for cascade reduction of 3-picoline.[a]

Entry	Cat. Loading / %	Solvent	HBpin equivalent	H$_2$ pressure / bar	Yield / %
1	0.2 mol% Ti$_3$-BPDC-CoH	Octane	1.05	20	97
2[b]	0.2 mol% Ti$_3$-BPDC-CoCl	Octane	1.05	20	0
3[c]	0.6 mol% Ti$_3$-BPDC	Octane	1.05	20	0
4[d]	0.2 mol% Co-NPs	Octane	1.05	20	0
5[e]	2 mol% NaBEt$_3$H	Octane	1.05	20	0

[a]Reaction conditions: Ti$_3$-BPDC-CoH (1 μmol Co) or other catalyst, 0.5 mmol 3-picoline, 0.525 mmol pinacolborane, 20 bar H$_2$, 1 mL Octane, 100 ºC, 22 hrs; Yield was determined by GC-MS analysis, mesitylene as internal standard. [b]Ti$_3$-BPDC-CoCl (1 μmol Co), as prepared above, was used as catalyst without further treatment. [c]Ti$_3$-BPDC (3 μmol Ti), as prepared above, was used as catalyst without further

treatment. [d]Co-NPs (1 µmol Co, black solid), generated by treating 1 µmol CoCl$_2$ (20 mM in THF) with 10 equiv. of NaBEt$_3$H for 1 hour and washed 3 times with toluene, was used as catalyst. [e]NaBEt$_3$H (10 µmol, 1.0 M in Hexane) was used as catalyst without further treatment.

5.3 A Typical Procedure for Ti$_3$-BPDC-CoH Catalyzed Cascade Reduction of Pyridines (Table 1).
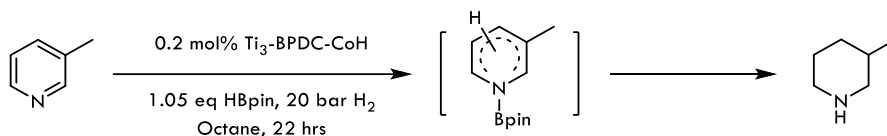
In a nitrogen-filled glovebox, Ti$_3$-BPDC-CoCl (2.0 mg, 1.0 µmol Co) in 1.0 mL toluene was charged into a glass vial. NaBEt$_3$H (10 µL, 1.0 M in Toluene) was added to the vial and the mixture was stirred for 1 hour. The solid was then centrifuged, washed with toluene three times, and washed with octane twice, before being transferred into a Parr reactor with 1 mL octane. 3-Picoline (49 µL, 0.50 mmol) and pinacolborane (77 µL, 0.525 mmol) was then added to the solution. The Parr reactor was sealed under nitrogen and charged with hydrogen to 20 bar. After stirring at 100 °C for 22 hours, the pressure was released and the MOF catalyst was removed from the reaction mixture via centrifugation. After being quenched with 2 drops of methanol, the supernatant was analyzed by GC-MS to give 3-methylpiperidine in 97% yield. 0.4% of Co leaching was determine by ICP-MS analysis of the organic extract from the reaction mixture, indicating minimal MOF decomposition during catalysis.
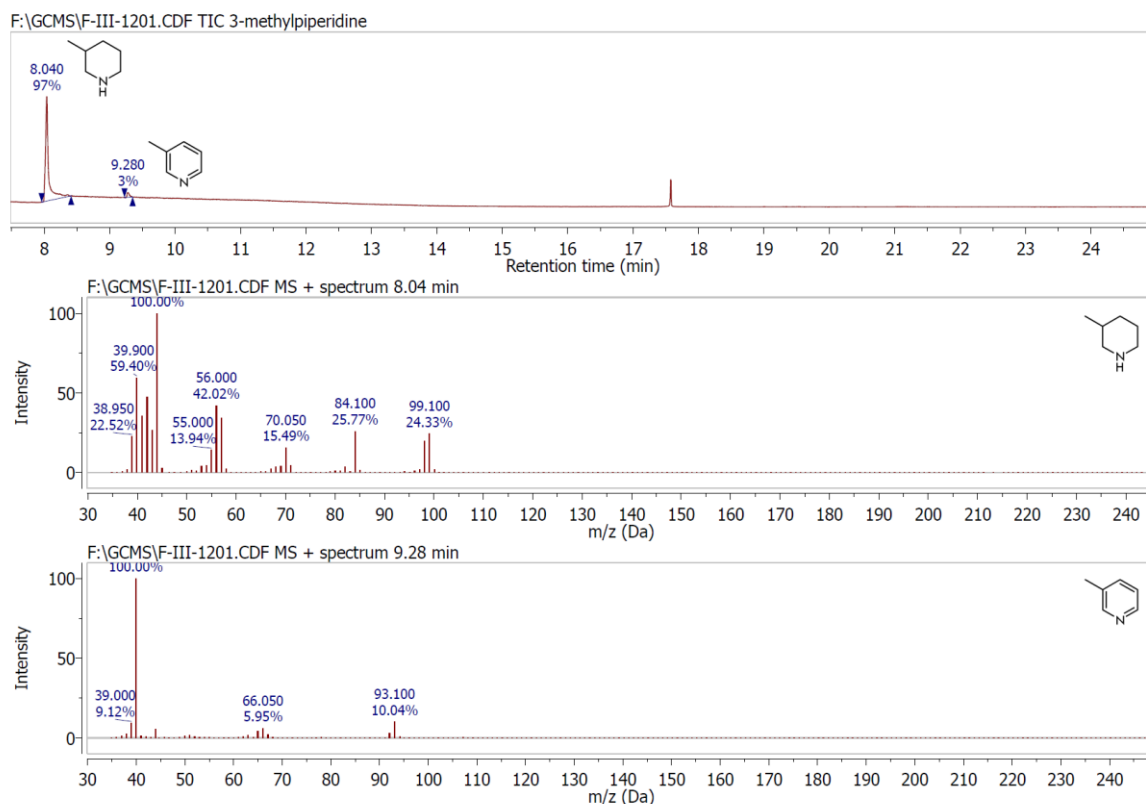
Figure S29. GC-MS spectrum of cascade reduction of 3-picoline to afford 3-methylpiperidine.

5.4 Reduction Pathway Study

Despite the fact that Ti$_3$-BPDC-CoH can catalyzed the hydroboration of 3-picoline in the absence of H$_2$ (Entry 3, Table S9), further experiments were conduct to demonstrate the whole cascade reduction pathway. As shown in Figure S30, hydroboration products of pyridine and 6-methoxyquinoline were prepared separately (see SI 5.1.2) and used as starting materials in the second step of catalytic hydrogenation. **Without adding any HBpin**, hydroboration products of pyridine and 6-methoxyquinoline can be fully hydrogenated to give piperidine and 1,2,3,4s-tetrahydro-6-methoxyquinoline in quantitive yield under 0.5 mol% of Ti$_3$-BPDC-CoH, 20 bar H$_2$ and 100 $^\circ$C. Background reaction without adding MOF resulted in no conversion and fully recovery of pyridine and 6-methoxyquinoline after hydrolysis under air. Such result proved that after the hydroboration of *N*-heteroarenes catalyzed by Ti$_3$-BPDC-CoH, the hydroborated products were

readily to undergo catalytic direct hydrogenation of the remaing unsaturated bonds to afford the fully reduced *N*-heterocycles. The above evidents strongly support our propose of cascade pathway in the reduction process of *N*-heteroarenes.
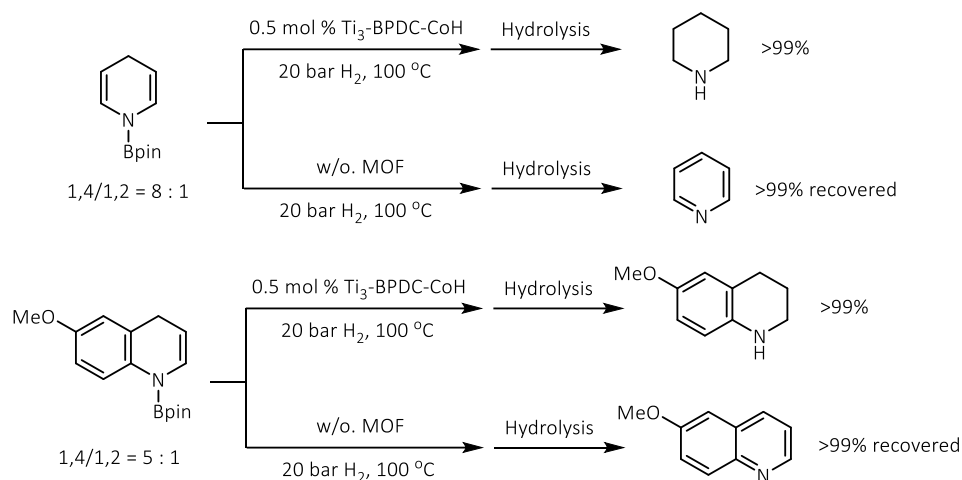
Figure S30. Control experiment using hydroborated pyridine and quinoline as starting materials.[20] The yield is based on GC-MS using mesitylene as internal standard.

5.5 Recycling Experiment
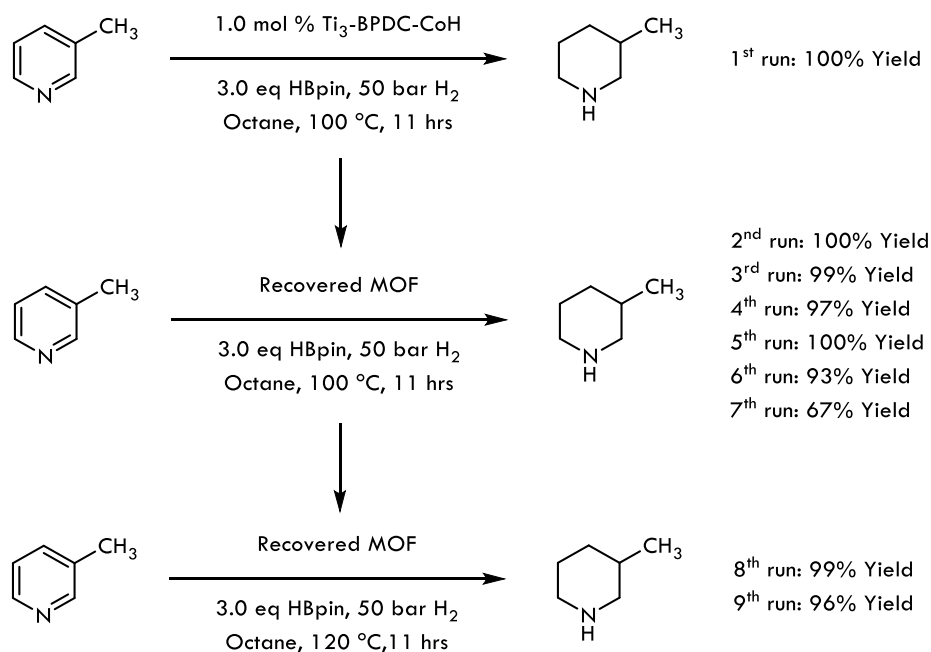
Figure S31. Recycle experiment of Ti$_3$-BPDC-CoH for the cascade reduction of 3-picoline.

In a nitrogen-filled glovebox, Ti_3-BPDC-CoCl (10.0 mg, 5.0 µmol Co) in 1.0 mL toluene was charged into a glass vial. $NaBEt_3H$ (50 µL, 1.0 M in toluene) was added to the vial and the mixture was stirred for 1 hour. The solid was then centrifuged, washed with toluene three times, and washed with octane twice, before being transferred into a Parr reactor with 1 mL octane. 3-Picoline (49 µL, 0.50 mmol) and pinacolborane (219 µL, 1.50 mmol) were then added to the solution. The Parr reactor was sealed under nitrogen and charged with hydrogen to 50 bar. After stirring at 100 °C for 11 hours, the pressure was released and the MOF catalyst was removed from the reaction mixture via centrifugation. The supernatant was transferred to a vial, and the MOF was washed with octane for later use. After being quenched with 2 drops of methanol, the supernatant was analyzed by GC-MS to give 3-methylpiperidine in 100% yield. The recovered solid catalyst was used for subsequent cycles of reactions. The reaction mixture of 3-picoline (49 µL, 0.50 mmol), pinacolborane (219 µL, 1.50 mmol), and the recovered MOF in 1 mL of octane was stirred for 11 hours in each run. Starting from thr 8th run, the reaction temperature was increased to 120 °C.
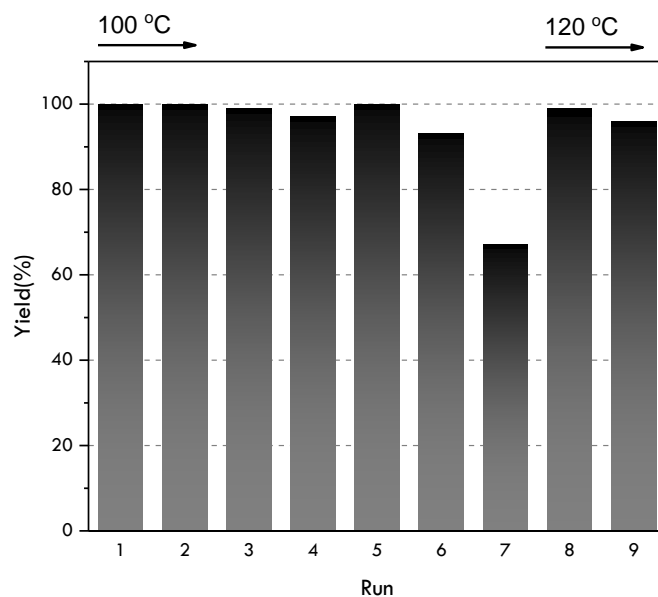
Figure S32. Plots of yields (%) of 3-methylpiperidine in six consecutive runs of Ti_3-BPDC-CoH catalyzed cascade reducation of 3-picoline. The Co-loadings were 1.0 mol%.

We also performed incomplete yield recycle experiments with a low Ti$_3$-BPDC-CoH catalyst loading of 0.5 mol% and a short reaction time of 5 h. No significant decrease in catalyst activity was observed in three runs (1st run: 68%; 2nd run: 53%; 3rd run: 58%).
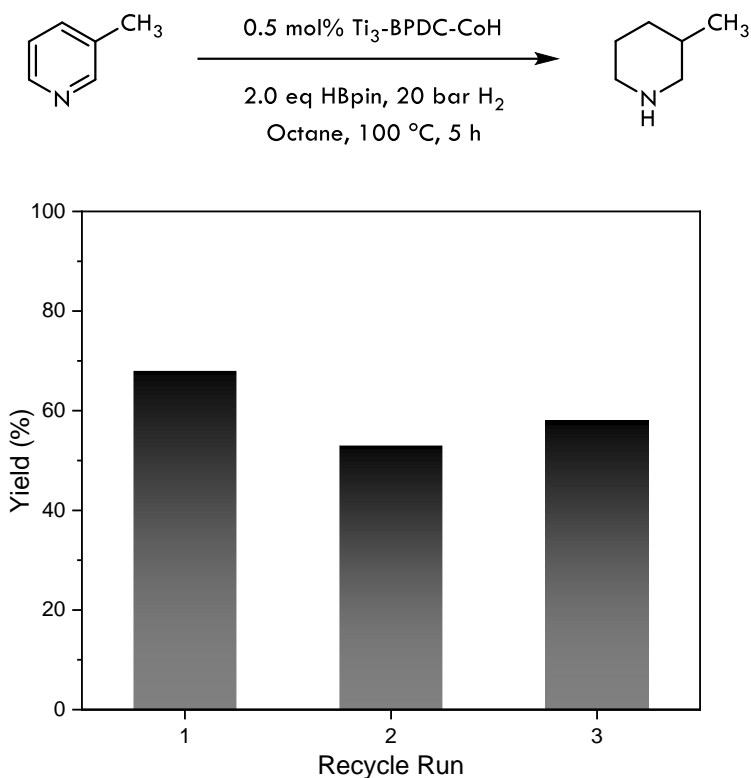
Figure S33. Plots of yields (%) of 3-methylpiperidine in three consecutive runs of Ti$_3$-BPDC-CoH catalyzed cascade reducation of 3-picoline. The Co-loadings were 0.5 mol%. Reaction condition: 0.5 mol% catalyst loading, 20 bar H$_2$, 2.0 eq HBpin, 1 mL Octane as solvent, 100 °C, 5 h.

5.6 Hot Filtration Test

"Hot Filtration" test was performed to rule out the possibility of leached Co species contributing to the cascade reduction reactivity. Specifically, 0.5 mol% of Ti$_3$-BPDC-CoH was first used to catalyze cascade reduction of quinolines to give 1,2,3,4-tetrahydroquinoline in >99% yield. Then, the MOF and supernatant were separated in a glovebox and used as catalysts for the cascade reduction of 3-picoline without any treatment. The recovered Ti$_3$-BPDC-CoH catalyst

afforded 3-methylpiperidine in 93% yield, while no conversion was detected in the reaction catalyzed by the supernatant. This experiment showed that the true catalytic species is MOF-supported Co-H but not leached Co species in the supernatant.
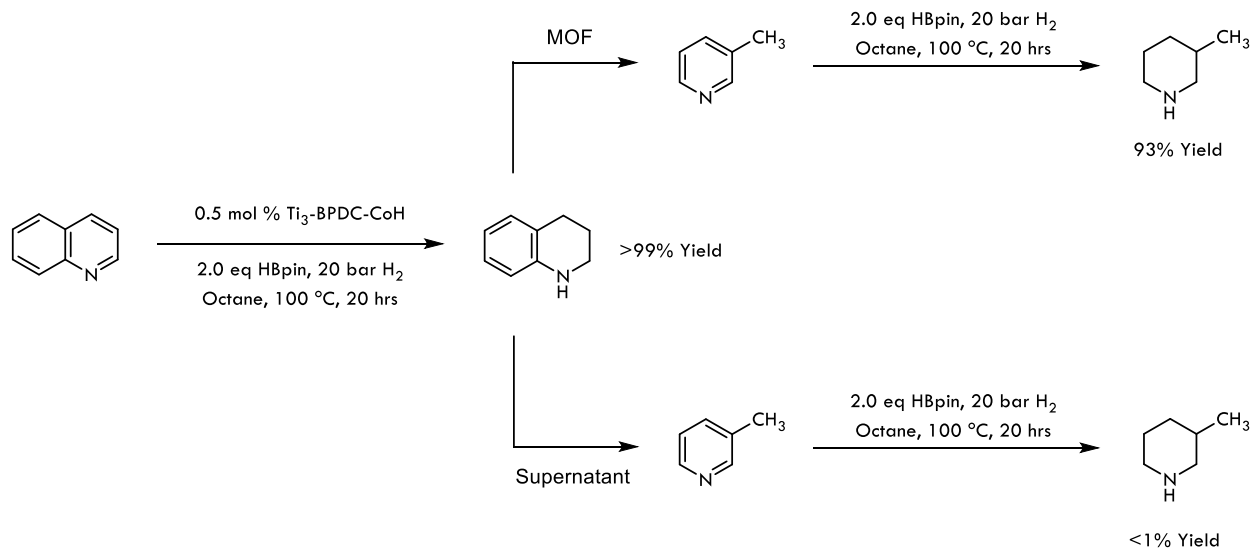
Figure S34. The "Hot Filtration" test of Ti$_3$-BPDC-CoH catalyzed cascade reduction of *N*-heteroarenes.

5.7 Screen for Broader Substrate Scope for Ti$_3$-BPDC-CoH Catalyzed Cascade Reduction of Pyridines

Beside the substrates shown in Table 1, several other pyridine derivaties have also been tested under standard or optimized conditions in Ti$_3$-BPDC-CoH catalyzed cascade reduction. The yields of different products were determined by GC-MS analysis.

As shown in Figure S35, boronic esters, amino groups and fluoride are tolerated under reaction conditions, although the product yields range from good to moderate. The reactive alkynyl group on the substrate was also fully hydrogenated under the cascade reduction reaction conditions.
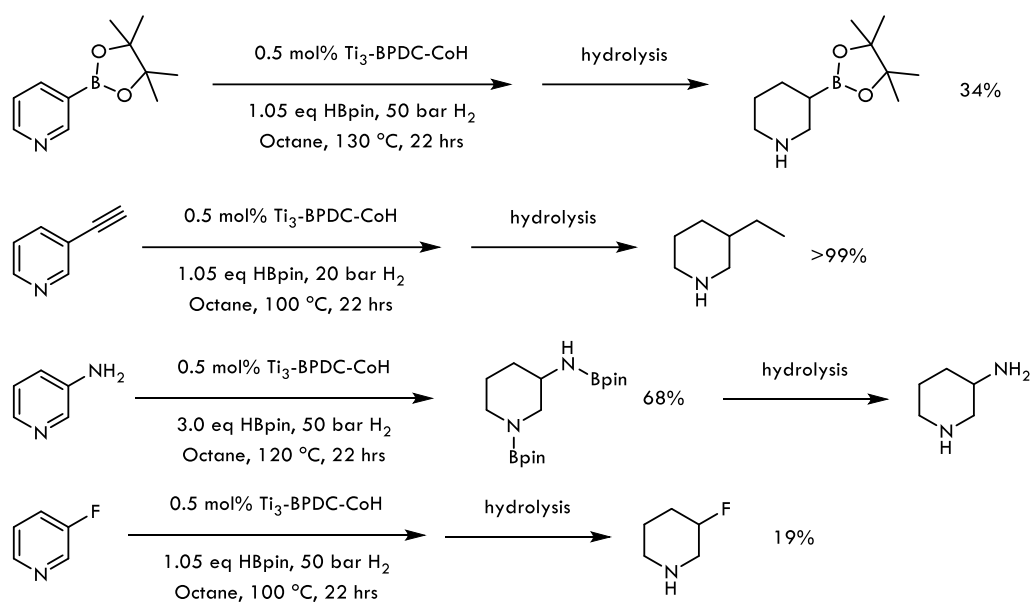
Figure S35. Additional substrate scope screening for Ti$_3$-BPDC-CoH catalyzed cascade reduction.

5.8 Reactivity Comparison with UiO-68-CoH

The catalytic activity of the present Co-H species supported by two neighboring SBUs in Ti$_3$-BPDC-CoH was compared to that in the previously reported UiO-68-CoH catalyst.[21] As shown in Table S11, while 0.2 mol% of Ti$_3$-BPDC-CoH catalyzed the cascade reduction of 3-picoline to 3-methylpiperidine in 97% yield, only 4% of the product was detected when the recation was carried out using UiO-68-CoH at a higher loading of 0.5%. We attribute such a dramatic difference in catalytic performance to their different anchoring modes. In UiO-68-CoH, each Co-H complex was supported by one Zr$_3$O$^-$ and Co centers can leach into the solution by strongly coordinating *N*-heteroarene to form inactive or less active Co nanoparticles. In contrast, Ti$_3$-BPDC provides two neighboring Ti-O$^-$ sites to chelate the Co-H complex, leading to a more robust catalyst. ICP-MS analyses showed that only 0.4% Co leached from Ti$_3$-BPDC-CoH after catalysis while nearly half of the Co species had leached from UiO-68-CoH under the same condition.

Table S11. Cascade Reduction Activity Comparison between Ti$_3$-BPDC-CoH and UiO-68-CoH.[a]
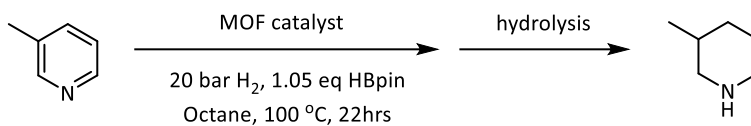
Catalyst	Yield of 3-methylpiperidine / %	Co Leaching after Reaction / %
0.2 mol% Ti₃-BPDC-CoH	97	0.4
0.5 mol% UiO-68-CoH	4	42.3

[a]Reaction conditions: Ti$_3$-BPDC-CoH (1 μmol Co) or UiO-68-CoH (2.5 μmol Co), 0.5 mmol 3-picoline, 0.525 mmol pinacolborane, 20 bar H$_2$, 1 mL Octane, 100 °C, 22 hrs; Yield was determined by GC-MS analysis, mesitylene as internal standard.

6. Ti₃-BPDC-CoH Catalyzed Selective Reduction of Quinolines

A Typical Procedure for Ti₃-BPDC-CoH Catalyzed Selective Reduction of Quinolines (Table 2).
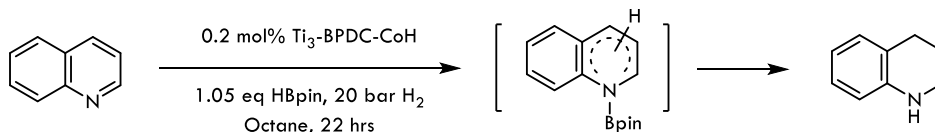
In a nitrogen-filled glovebox, Ti$_3$-BPDC-CoCl (2.0 mg, 1.0 μmol Co) in 1.0 mL toluene was charged into a glass vial. NaBEt$_3$H (10 μL, 1.0 M in toluene) was added to the vial and the mixture was stirred for 1 hour. The solid was then centrifuged, washed with toluene three times, and washed with octane twice, before being transferred into a Parr reactor with 1 mL octane. Quinoline (59 μL, 0.50 mmol) and pinacolborane (77 μL, 0.525 mmol) were then added to the solution. The Parr reactor was sealed under nitrogen and charged with hydrogen to 20 bar. After stirring at 100 °C for 22 hours, the pressure was released and the MOF catalyst was removed from the reaction mixture via centrifugation. After being quenched with 2 drops of methanol, the supernatant was analyzed by GC-MS to selectively give 1,2,3,4-tetrahydroquinoline in 98% yield along with a trace amount (< 2%) of 5,6,7,8-tetrahydroquinoline and decahydroquinoline.
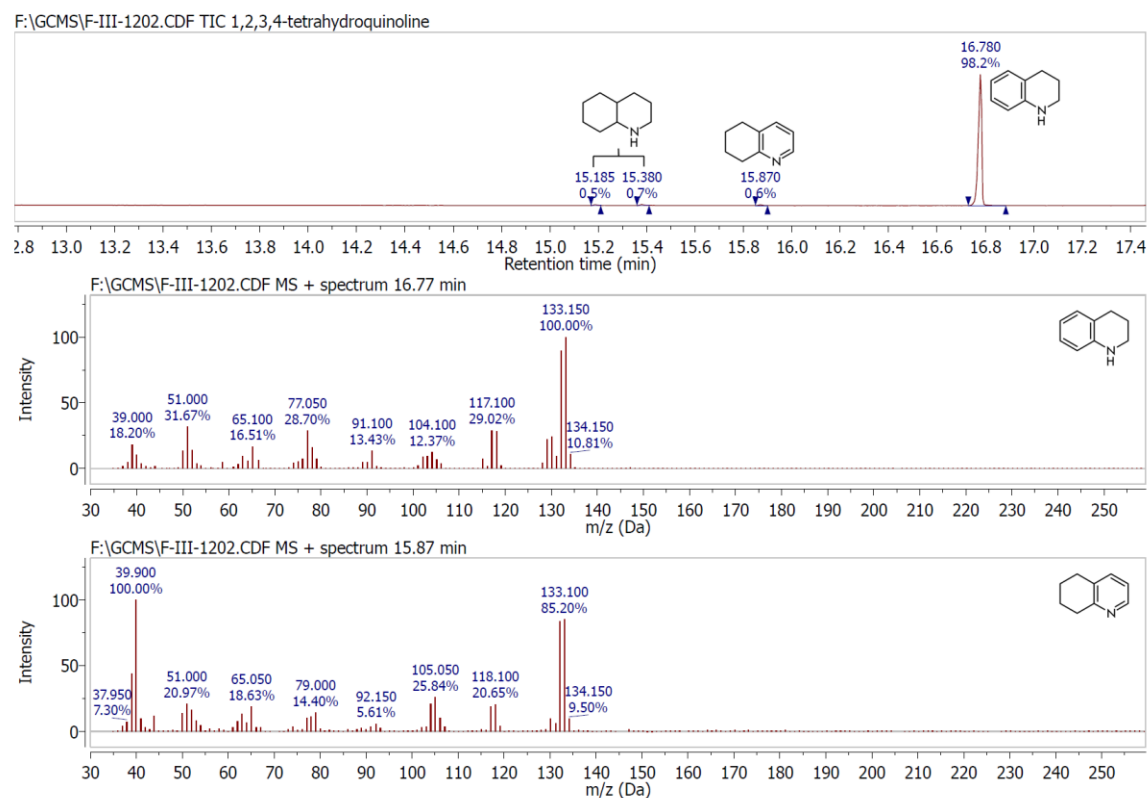
Figure S36. GC-MS spectrum of selective reduction of quinoline to afford 1,2,3,4-tetrahydroquinoline.

7. GC-MS Analysis

The conversions of reactions were determined by GC-MS using a Shimadzu GCMS-QP2010 Ulta. Column: SH-Rxi-5Sil MS column, 30.0 m in length, 0.25 mm in diameter, 0.25 μm in thickness. GC conditions: Injection temperature, 220 °C; Column temperature program, 30 °C hold for 5 min, followed by a ramp of 5 °C/min to 60 °C then a ramp of 20 °C/min to 300 °C; Column flow, 1.21 mL/min.

Table S12. The retention times of GC traces I (some compounds have multiple stereoisomers, thus showing more than one peak with the expected molecular mass).

Compound	Retention Time	Compound	Retention Time
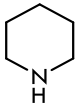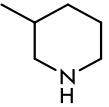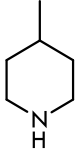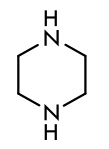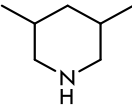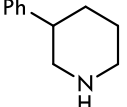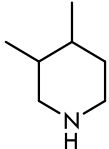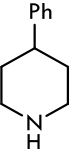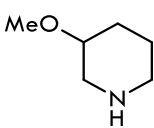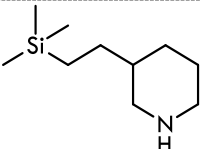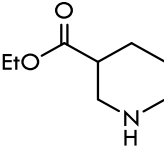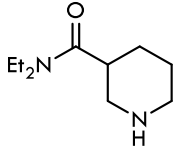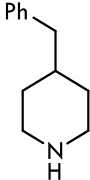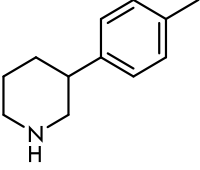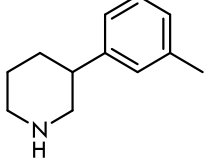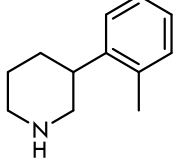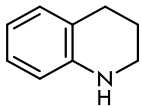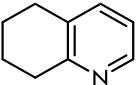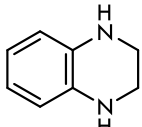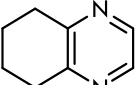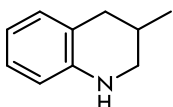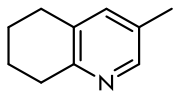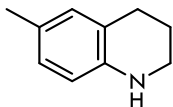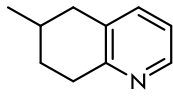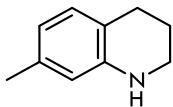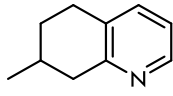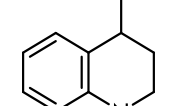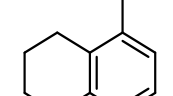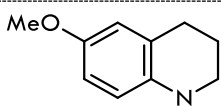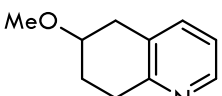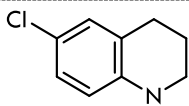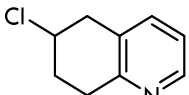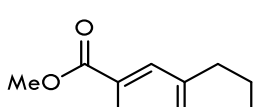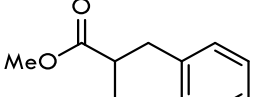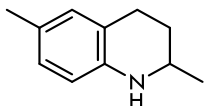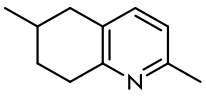
Compound	Retention Time	Compound	Retention Time
piperidine	5.271 min	3-methylpiperidine	8.037 min
4-methylpiperidine	7.851 min	piperazine	9.133 min
3,5-dimethylpiperidine	10.445 min; 10.755 min	3-phenylpiperidine	17.514 min
3,4-dimethylpiperidine	11.055 min; 11.700 min	4-phenylpiperidine	17.499 min
3-methoxypiperidine	12.591 min	3-(2-(trimethylsilyl)ethyl)piperidine	16.319 min
ethyl piperidine-3-carboxylate	15.852 min	N,N-diethylpiperidine-3-carboxamide	18.208 min
4-benzylpiperidine	18.104 min	3-(4-methylphenyl)piperidine	N.D.
3-(3-methylphenyl)piperidine	18.179 min	3-(2-methylphenyl)piperidine	18.199 min

Table S13. The retention times of GC traces II.

Compound	Retention Time	Compound	Retention Time
1,2,3,4-tetrahydroquinoline	16.735 min	5,6,7,8-tetrahydroquinoline	15.870 min
1,2,3,4-tetrahydroquinoxaline	17.938 min	5,6,7,8-tetrahydroquinoxaline	15.750 min

	17.140 min		16.811 min
	17.471 min		N.D.
	17.572 min		N.D.
	17.208 min		17.008 min
	18.438 min		17.309 min
	18.503 min		N.D.
	20.363 min		18.532 min
	N.D.		N.D.

8. References

1. M. Dan-Hardi, C. Serre, T. Frot, L. Rozes, G. Maurin, C. Sanchez and G. Férey, *J. Am. Chem. Soc.*, 2009, **131**, 10857-10859.
2. J. Gao, J. Miao, P.-Z. Li, W. Y. Teng, L. Yang, Y. Zhao, B. Liu and Q. Zhang, *Chem. Commun.*, 2014, **50**, 3786-3788.
3. B. Bueken, F. Vermoortele, D. E. Vanpoucke, H. Reinsch, C. C. Tsou, P. Valvekens, T. De Baerdemaeker, R. Ameloot, C. E. Kirschhock and V. Van Speybroeck, *Angew. Chem. Int. Ed.*, 2015, **54**, 13912-13917.
4. J. A. Mason, L. E. Darago, W. W. Lukens Jr and J. R. Long, *Inorg. Chem.*, 2015, **54**, 10096-10104.
5. S. Yuan, T.-F. Liu, D. Feng, J. Tian, K. Wang, J. Qin, Q. Zhang, Y.-P. Chen, M. Bosch, L. Zou, S. J. Teat, S. J. Dalgarno and H.-C. Zhou, *Chem. Sci.*, 2015, **6**, 3926-3930.

6.   H. Assi, L. C. Pardo Pérez, G. Mouchaham, F. Ragon, M. Nasalevich, N. Guillou, C. Martineau, H. Chevreau, F. Kapteijn and J. Gascon, *Inorg. Chem.*, 2016, **55**, 7192-7199.

7.   H. L. Nguyen, F. Gándara, H. Furukawa, T. L. Doan, K. E. Cordova and O. M. Yaghi, *J. Am. Chem. Soc.*, 2016, **138**, 4330-4333.

8.   H. L. Nguyen, T. T. Vu, D. Le, T. L. Doan, V. Q. Nguyen and N. T. Phan, *ACS Catal.*, 2016, **7**, 338-342.

9.   S. Wang, T. Kitao, N. Guillou, M. Wahiduzzaman, C. Martineau-Corcos, F. Nouar, A. Tissot, L. Binet, N. Ramsahye and S. Devautour-Vinot, *Nat. Commun.*, 2018, **9**.

10.   Y. Keum, S. Park, Y.-P. Chen and J. Park, *Angew. Chem. Int. Ed.*, 2018, DOI: doi:10.1002/anie.201809762, doi:10.1002/anie.201809762.

11.   K. Hong and H. Chun, *Inorg. Chem.*, 2013, **52**, 9705-9707.

12.   T. Yang, S.-j. Park, T. G. Kim, D. S. Shin and J. Park, *Opt. Express*, 2017, **25**, 30843-30850.

13.   C. Xie, S. Yang, J. Shi and C. Niu, *Catalysts*, 2016, **6**, 117.

14.   H. Belhadj, A. Hakki, P. K. J. Robertson and D. W. Bahnemann, *Phys. Chem. Chem. Phys.*, 2015, **17**, 22940-22946.

15.   H. Sheng, H. Zhang, W. Song, H. Ji, W. Ma, C. Chen and J. Zhao, *Angew. Chem. Int. Ed.*, 2015, **54**, 5905-5909.

16.   J. J. Rehr and R. C. Albers, *Rev. Mod. Phys.*, 2000, **72**, 621.

17.   B. Ravel and M. Newville, *J. Synchrotron. Rad.*, 2005, **12**, 537-541.

18.   F. Dai, Q. Gui, J. Liu, Z. Yang, X. Chen, R. Guo and Z. Tan, *Chem. Commun.*, 2013, **49**, 4634-4636.

19.   S. Thapa, S. K. Gurung, D. A. Dickie and R. Giri, *Angew. Chem. Int. Ed.*, 2014, **53**, 11620-11624.

20.   P. Ji, X. Feng, S. S. Veroneau, Y. Song and W. Lin, *J. Am. Chem. Soc.*, 2017, **139**, 15600-15603.

21.   K. Manna, P. Ji, Z. Lin, F. X. Greene, A. Urban, N. C. Thacker and W. Lin, *Nat. Commun.*, 2016, **7**, 12610.